Synoptic and Mesoscale Processes Supporting Vertical Superposition of the Polar and Subtropical Jets in Two Contrasting Cases

By

ANDREW C. WINTERS[1] and JONATHAN E. MARTIN[2*]

[1]Department of Atmospheric and Environmental Sciences
University at Albany – State University of New York
Albany, NY 12222

[2]Department of Atmospheric and Oceanic Sciences
University of Wisconsin-Madison
Madison, WI 53706

Keywords: Jet Streams; Ageostrophic Transverse Circulations; Convection
Running Head: Processes Supporting Jet Superposition

Submitted for publication in the *Quarterly Journal of the Royal Meteorological Society*
17 September 2015

[*] *Corresponding author address:* Jonathan E. Martin, Dept. of Atmospheric and Oceanic Sciences, University of Wisconsin-Madison, 1225 W. Dayton St., Madison, WI 53706. E-mail: jemarti1@wisc.edu

Abstract

Observational studies have shown that the tropopause characteristically exhibits a three-step pole-to-equator structure, with each break between steps in the tropopause height associated with a jet stream. While the two jet streams, the polar and subtropical jets, typically occupy different latitude bands, their separation can occasionally vanish, resulting in a relatively rare vertical superposition of the two jets. A cursory examination of several historical and recent high-impact weather events over North America and the North Atlantic suggests that superposed jets are a component of their evolution. This study examines the processes that support the production of a polar/subtropical jet superposition during two such events; the 18–20 December 2009 Mid-Atlantic Blizzard and the 1–3 May 2010 Nashville Flood.

Given that ageostrophic transverse circulations and convection have both been shown to be capable of restructuring the tropopause within a single jet environment, the analysis focuses on the role these same processes play within the more complex double jet environment. The results demonstrate that ageostrophic transverse circulations play a primary role in the production of a superposition during the December 2009 case by placing subsidence, and a downward protrusion of high potential vorticity (PV) air, between the two jet cores, thereby contributing to the production of the single, steep tropopause wall characteristic of the superposed jet environment. Furthermore, convection fundamentally influences the existence and structure of the subtropical jet stream in both cases, through its associated latent heat release and irrotational outflow as well as the geostrophic adjustment process that responds to upper-tropospheric mass deposition from convection on the anticyclonic shear side of the jet.

1. Introduction

Narrow, rapidly flowing currents of air located near the tropopause are known as jet streams or jets. These jets, often found nearly girdling the globe while exhibiting large meridional meanders, are among the most recognizable structural characteristics within the Earth's atmosphere. Careful observational work by Defant and Taba (1957, hereafter DT57) was one of the first to demonstrate that the location of these jets is intricately related to the structure of the tropopause. Specifically, they found that the atmosphere typically exhibits the three-step pole-to-equator tropopause structure[1] shown in Fig. 1, wherein each step is separated from its neighbors by the presence of a westerly wind maximum (Winters and Martin 2014, their Fig. 2). In particular, the subtropical jet resides within the break between the tropical (~90 hPa) and subtropical tropopause (~250 hPa) at the poleward edge of the Hadley cell and is characterized by relatively modest baroclinicity in the upper troposphere and lower stratosphere (e.g., Loewe and Radok 1950; Yeh 1950; Koteswaram 1953; Mohri 1953; Koteswaram and Parthasarathy 1954; Sutcliffe and Bannon 1954; Krishnamurti 1961; Riehl 1962). The polar jet is located farther poleward (~50^{o}N) in the break between the subtropical tropopause and the even lower polar tropopause (~300 hPa) and is positioned atop the strongly baroclinic, tropospheric-deep polar front (e.g., Palmén and Newton 1948; Namias and Clapp 1949; Newton 1954; Palmén and Newton 1969; Keyser and Shapiro 1986; Shapiro and Keyser 1990).

A particularly insightful element of the DT57 analysis was their construction of hemispheric maps of tropopause height (in hPa). One such map, shown in Fig. 2 (Winters and Martin 2014, their Fig. 3), demonstrates that the location of the individual tropopause breaks, and thus the jets at any particular time, are characterized by sharp, localized, and easily identifiable

[1] DT57 identified the tropopause via the analysis of soundings. The tropopause was identified at the elevation of a "noticeable change of tropospheric lapse rate to an isothermal layer or to an increase of temperature with height." (DT57, p. 261)

94 gradients in tropopause height. While the analysis indicates that the polar and subtropical jets
95 typically occupy different latitude bands, substantial meanders in their location are common.
96 Occasionally, the characteristic meridional separation between the two jets can vanish, as it does
97 in Fig. 2 in the area bounded by the black circle over the North Atlantic, where the polar and
98 subtropical jets vertically superpose.[2] The consequences of such a vertical superposition are the
99 development of a two-step tropopause structure from the tropics to high latitudes, rather than the
100 more common three-step structure represented in Fig. 1, and a consolidation of the upper-
101 tropospheric and lower-stratospheric baroclinicity associated with each jet into a substantially
102 narrower zone of contrast. Together, these observations of the tropopause by DT57 are
103 specifically identified as the theoretical foundation to an objective jet identification scheme
104 outlined in Winters and Martin (2014, hereafter WM14).
105 Employing that jet identification scheme as part of an analysis of the 1–3 May 2010
106 Nashville Flood, WM14 found that the event was characterized by the development of a
107 superposed jet. As the jets became superposed, WM14 diagnosed a strengthening of the
108 associated ageostrophic transverse circulation. The low-level, poleward-directed branch of this
109 circulation was subsequently found to make the primary contribution to an observed increase in
110 poleward moisture flux over the southeastern United States that preceded the second day of
111 heavy rainfall characterizing the 2010 Nashville Flood. Moore et al. (2012) indicated that this
112 increase in poleward moisture flux was essential for the continued production of heavy
113 precipitation during the latter half of the event. In light of this result, the analysis by WM14

[2] More recently, potential vorticity (PV) tropopause maps have also been beneficial in locating the individual tropopause breaks and the occasional vertical superposition of the polar and subtropical jets (e.g., Hoskins and Berrisford 1988; Davis and Emanuel 1991; Hakim et al. 1995; Bosart et al. 1996; Morgan and Nielsen-Gammon 1998; Shapiro et al. 1999).

114 highlighted one specific pathway through which a superposed jet, and its associated ageostrophic
115 transverse circulation, can influence the evolution of a high-impact weather event.
116 In addition to the 2010 Nashville Flood, a cursory examination of a number of other
117 historical and recent high-impact weather events over North America and the North Atlantic by
118 the authors suggests that superposed jets were a component of their evolution. For example,
119 Defant (1959) discussed the impact of a dramatic jet superposition on an explosive cyclogenesis
120 event south of Iceland on 8 January 1956, in which the sea level pressure dropped 61 hPa in 24
121 h. Furthermore, the 25–26 January 1978 Cleveland Superbomb (Hakim et al. 1995, their Fig. 5),
122 the 15–16 October 1987 Great October Storm (Hoskins and Berrisford 1988, their Fig. 7), the
123 12–14 March 1993 Storm of the Century (Bosart et al. 1996, their Fig. 13), the 18–20 December
124 2009 Mid-Atlantic Blizzard (National Weather Service 2014), and the 25–28 April 2011 severe
125 weather outbreak (Christenson and Martin 2012) are all examples of events that occurred within
126 an environment that exhibited the two-step tropopause structure associated with a superposed jet.
127 The association of jet superpositions with a class of high-impact weather events, and the
128 relatively infrequent occurrence of superpositions over North America and the North Atlantic
129 (Christenson 2013), motivates an investigation into the mechanisms that support the process of
130 superposition. This topic was not considered as part of the previous work by WM14 and remains
131 an out standing research question. Historically, prior work that addresses the related topic of jet
132 “mergers” has been focused on either interannual or climatological time scales (e.g., Lee and
133 Kim 2003; Son and Lee 2005; Eichelberger and Hartmann 2007; Harnik et al. 2014), has been
134 strongly based on wave-wave interaction (e.g., Lee and Kim 2003; Son and Lee 2005; Martius et
135 al. 2010; O’Rourke and Vallis 2013), and/or has been conducted within an idealized model
136 environment (e.g., Lee and Kim 2003; Son and Lee 2005; O’Rourke and Vallis 2013). This

circumstance, coupled with only limited analysis of such features using actual observed data, has resulted in incomplete insight into the synoptic-dynamic mechanisms that foster the development of jet superpositions.

The concept of mid-latitude trough mergers (e.g., Lai and Bosart 1988; Gaza and Bosart 1990; Hakim et al. 1995; Hakim et al. 1996; Dean and Bosart 1996; Strahl and Smith 2001), in which two mid-tropospheric vorticity maxima with origins in distinctly different westerly airstreams amalgamate into a single maximum, offers the closest physical analog to jet superpositions in the synoptic-dynamic literature. These studies emphasize that trough merger often results in explosive cyclogenesis – also a frequent by-product of jet superposition. While it appears that certain trough merger cases may be simultaneously characterized by jet superpositions, the aforementioned studies do not identify the merging air streams as distinctly related to separate polar and subtropical jets and do not specifically investigate the impact of trough merger on the evolution of the upper-tropospheric jet and tropopause structure. Instead, the focus of these studies is largely placed on the effects merger can have on the development of surface cyclones.

Numerous observationally based studies have addressed the different mechanisms that can be responsible for altering the structure of an *individual* jet stream, however. For instance, the presence of ageostrophic transverse circulations, and particularly the differential vertical motions associated with them, in the vicinity of an upper-level jet-front system can act not only to aid in the production of precipitation, but also to significantly restructure the baroclinicity and tropopause both above and below the jet. Many of the historical contributions to the problem of upper-tropospheric frontogenesis are well summarized by Keyser and Shapiro (1986), while

159 Lang and Martin (2012) provide a recent extension of these studies to the process of lower-
160 stratospheric frontogenesis.

161 The influence of convection in altering the structure of the tropopause on the anticyclonic
162 shear side of a jet has also been well documented. In particular, Lang and Martin (2013)
163 investigated four cases of upper-frontal evolution in southwesterly flow. They noted that latent
164 heat release offers separate but simultaneous physical mechanisms that can alter the tropopause
165 structure. First, direct diabatic erosion of potential vorticity (PV) above the heating maximum
166 can increase the tropopause height in a given column. Second, the associated reduction in upper-
167 tropospheric static stability can intensify a forced ageostrophic transverse circulation, which can
168 then act to further tilt the tropopause. Tropical cyclones and extratropical transition (ET) events
169 have also been shown to exert a considerable influence on the location and strength of the
170 subtropical jet via the negative PV advection accomplished by their tropopause-level, divergent
171 outflow and the diabatic erosion of upper-tropospheric PV that accompanies intense latent heat
172 release in the middle troposphere (e.g., Ahmadi-Givi et al. 2004; Agusti-Panareda et al. 2004;
173 McTaggart-Cowan et al. 2001; McTaggart-Cowan et al. 2004; McTaggart-Cowan et al. 2007;
174 Grams et al. 2011; Grams et al. 2013; Archambault et al. 2013; Griffin and Bosart 2014;
175 Archambault et al. 2015).

176 Despite extensive research on a variety of aspects of upper-level jet-front systems, no
177 prior study has examined the role of the above dynamical mechanisms in specifically supporting
178 the interaction and subsequent vertical superposition of the two, initially distinct, jet features.
179 Consequently, the present study will consider the specific roles that ageostrophic transverse
180 circulations, convection, and the interaction between the two may play in the restructuring of the
181 tropopause that characterizes jet superpositions. These objectives stand in contrast to WM14,

which focused solely on the specific role that a superposed jet's ageostrophic transverse circulation played in magnifying a high-impact event. The process of superposition will be addressed through the examination of two recent high-impact weather events associated with superposed jets: the 18–20 December 2009 Mid-Atlantic Blizzard and the aforementioned 1–3 May 2010 Nashville Flood. These events were selected because they occurred at different times of the year and were associated with different types of high-impact weather events (i.e., rapid cyclogenesis and an extreme precipitation event).

The remainder of this study is structured as follows. Section 2 briefly discusses the WM14 jet identification scheme, given its relevance to the current study, and provides some background on the Sawyer-Eliassen circulation equation (Sawyer 1956; Eliassen 1962), which is used to diagnose the ageostrophic transverse jet circulations. Sections 3 and 4 diagnose the development of a superposed jet during each individual case, respectively, and Section 5 finishes with a discussion and suggestions for future work.

2. Methodology

This study is performed using model analyses from the National Centers for Environmental Prediction (NCEP) Global Forecast System (GFS) at 6 h intervals with a horizontal grid spacing of 1.0^{o} x 1.0^{o} and a vertical grid spacing of 50 hPa (25 hPa between 1000 hPa and 900 hPa). To accommodate the jet identification scheme outlined in WM14, which is briefly summarized below, these data were bilinearly interpolated onto isentropic surfaces at 5-K intervals from 300–370-K using programs within the General Meteorological Package (GEMPAK; desJardins et al. 1991). Throughout the subsequent analysis, the tropopause will refer to the location of the 2-PVU surface (1 PVU = K m^2 kg^{-1} s^{-1}), in line with defining the dynamic tropopause as a surface of constant PV (e.g., Morgan and Nielsen-Gammon 1998).

205 With this definition for the dynamic tropopause, and in an effort to better diagnose its movement,
206 PV advection is calculated using only the gradient in the 1–3-PVU channel.

207 *2.1 Jet Identification*

208 The forthcoming summary of the identification scheme for the polar, subtropical, and
209 superposed jet streams[3] contains elements from WM14 and references the features shown in Fig.
210 3 (WM14, their Fig.4). Figure 3a depicts a characteristic example of clearly separate polar and
211 subtropical jets from 0000 UTC 27 April 2010 in the eastern North Pacific. A vertical cross
212 section from A-A' through these distinct features unambiguously identifies the separate jet cores
213 and a three-step tropopause structure (Fig. 3b). From this cross section, it is apparent that the
214 polar jet core, located at approximately 300 hPa, is largely contained within the 315–330-K
215 isentropic layer, while the subtropical jet core occupies the 340–355-K isentropic layer at
216 roughly 200 hPa. Additionally, both the polar and the subtropical jets lie at the low PV edge of
217 the strong horizontal PV gradient that separates the upper troposphere from the lower
218 stratosphere in their respective isentropic layers. With these attributes in mind, the identification
219 scheme identifies the presence, or absence, of a polar or subtropical jet within each grid column
220 based upon whether the wind speed distribution and horizontal PV gradient within each jet's
221 isentropic layer satisfy the criteria specified in WM14. The occurrence of both polar and
222 subtropical jet characteristics in a single grid column identifies a jet superposition at that time in
223 that grid column. An example of a jet superposition is shown in Fig. 3c at 0000 UTC 24 October
224 2010. Notice that, rather than the three-step tropopause structure shown in Fig. 3b, a superposed
225 jet is characterized by a two-step tropopause structure with a steep tropopause wall that extends

[3] Throughout the course of this study, the term jet "stream" is synonymous with jet "streak" and will refer to a zonally confined wind speed maximum along either the polar or subtropical waveguide.

from the polar to the tropical tropopause (Fig. 3d). This nearly vertical PV wall (from roughly 550 to 150 hPa in this example case) is the leading structural characteristic of a superposed jet.

2.2 Sawyer-Eliassen Circulation Equation

A particularly powerful diagnostic tool for interrogating the ageostrophic transverse circulations associated with jet-front structures, in nearly straight flow, is afforded by the Sawyer-Eliassen circulation equation (Sawyer 1956; Eliassen 1962)[4]:

$$(-\gamma\frac{\partial\theta}{\partial p})\frac{\partial^2\psi}{\partial y^2}+(2\frac{\partial M}{\partial p})\frac{\partial^2\psi}{\partial p\partial y}+(-\frac{\partial M}{\partial y})\frac{\partial^2\psi}{\partial p^2}=Q_g-\gamma\frac{\partial}{\partial y}(\frac{d\theta}{dt}) \qquad (1)$$

where γ is a constant on isobaric surfaces [$\gamma=(R/fp_o)(p_o/p)^{c_v/c_p}$], p_o=1000 hPa, c_v=718 J kg^{-1} K^{-1}, c_p=1004 J kg^{-1} K^{-1}, R is the gas constant for dry air, θ is the potential temperature, and f is the Coriolis parameter. In addition, Q_g is the geostrophic forcing term, which is the sum of the shearing { $Q_{SH}=2\gamma[(\partial U_g/\partial y)(\partial\theta/\partial x)]$ } and stretching deformation terms { $Q_{ST}=2\gamma[(\partial V_g/\partial y)(\partial\theta/\partial y)]$ } and where U_g and V_g are the along- and across-front geostrophic winds, respectively. M is defined as the absolute geostrophic momentum ($M=U_g-fy$). The coefficients of the second-order terms on the left-hand side of (1) represent the static stability, baroclinicity, and inertial stability, respectively, and act to modulate the structure of the ageostrophic transverse circulation. The ageostrophic transverse circulation lies in a plane perpendicular to the frontal boundary (i.e., jet axis) and is determined by the Sawyer-Eliassen streamfunction, ψ, such that the across-front ageostophic wind and vertical motion are defined as $v_{ag}=-\partial\psi/\partial p$ and $\omega=dp/dt=\partial\psi/\partial y$, respectively. In the solution, the along-front component of the ageostrophic circulation (u_{ag}) is assumed to be zero. For the purposes of this study, successive overrelaxation (SOR) is used to converge on a solution to (1) for the

[4] Eq. (1) is shown in isobaric coordinates, which offers the advantage of distinguishing between the geostrophic and diabatic forcing terms.

247 ageostrophic transverse circulation following the method described in WM14. The reader is
248 referred to Eliassen (1962) or Keyser and Shapiro (1986) for the full derivation and a more
249 detailed discussion of (1).

250 Employing (1), Shapiro (1982) described a series of conceptual models detailing the
251 characteristic transverse circulations associated with idealized upper-level jet-front systems.
252 Specifically, in the absence of any along-jet geostrophic temperature advection, solutions for the
253 ageostrophic circulations are driven purely by the geostrophic stretching deformation and
254 resembled the traditional four-quadrant model, with a thermally direct (indirect) circulation in
255 the jet-entrance (-exit) region (Fig. 4a). The introduction of along-jet geostrophic temperature
256 advection mobilizes the geostrophic shearing deformation term, which acts to "shift" the
257 thermally direct (indirect) circulation to the anticyclonic (cyclonic) shear side of the jet in cases
258 of geostrophic cold-air advection, such that subsidence is present through the jet core (Fig. 4b).
259 Conversely, geostrophic warm-air advection along the jet axis shifts the thermally direct
260 (indirect) circulation to the cyclonic (anticyclonic) shear side of the jet, positioning ascent
261 through the jet core (Fig. 4c)[5].

262 **3. Jet Evolution during the 18-20 December 2009 Mid-Atlantic Blizzard**

263 *3.1 Synoptic Overview*

264 Throughout the 72 h period of 18–20 December 2009, large portions of the Mid-Atlantic
265 and New England states accumulated 30-60 cm of snow in conjunction with a rapidly deepening
266 mid-latitude cyclone that formed over the northern Gulf of Mexico and tracked northeastward
267 along the East Coast (National Weather Service 2014). Coincident with the cyclone's most rapid
268 period of intensification was the development of a jet superposition over the southeastern United

[5] These circulations are fortified by ascent and descent associated with positive and negative vorticity advection by the thermal wind (i.e., Sutcliffe 1947) as described by Martin (2014).

States. For brevity, the following overview will focus primarily on the jet evolution in the upper troposphere in the hours preceding superposition.

At 0000 UTC 19 December, 36 h prior to jet superposition, a subtropical jet (red dashed line) with winds in excess of 60 m s^{-1} extended from central Mexico northeastward across the Florida peninsula, while a weaker polar jet (blue dashed line) was identified upstream of a polar trough in northwesterly flow over the Central Plains (Fig. 5a). A cross section through the two separate jet structures at this time (Fig. 5b) indicates the presence of a three-step tropopause structure and demonstrates that the jets were clearly distinct from one another. The developing mid-latitude cyclone responsible for producing blizzard conditions across much of the eastern United States was also firmly located in a favorable position for further deepening in the subtropical jet's left exit region.

By 1800 UTC 19 December, the subtropical jet was displaced slightly poleward of its previous location and was noticeably stronger, with winds now in excess of 80 m s^{-1} (Fig. 5c). The surface cyclone, which had deepened by roughly 8 hPa, remained favorably located within the subtropical jet's left exit region off of the Mid-Atlantic coast, suggesting that the jet likely played a role in the cyclone's development. Meanwhile, the polar jet, which was also characterized by increased wind speeds, had propagated around the base of the deepening polar trough and had assumed an orientation parallel to the subtropical jet over the southeastern United States. A cross section through the entrance regions of both of these jet structures (Fig. 5d) indicates the persistence of a three-step tropopause structure and that the two jets, while in closer proximity to one another by this time, were still not vertically superposed.

During the subsequent 18 h, the cyclone underwent its most rapid period of intensification, reaching a minimum central pressure below 980 hPa southeast of Cape Cod at

1200 UTC 20 December (Fig. 5e). Coincident with this period of most rapid intensification was a superposition of the polar and subtropical jets from central Georgia northeastward to off the North Carolina coast (yellow line). This superposed jet was characterized by increased wind speeds, now well in excess of 90 m s^{-1}, and was positioned such that the cyclone remained firmly located in the jet's left exit region. An investigation of the movement of each individual jet axis from the previous time indicates that the subtropical jet was, once again, displaced only slightly poleward of its prior location, while the polar jet was located farther southeast of its previous position, consistent with the continued propagation and deepening of the polar trough.

A cross section drawn through the superposed portion of this jet illustrates the two-step tropopause structure and vertical PV wall (extending from roughly 500 hPa to 150 hPa) characteristic of a superposed jet (Fig. 5f). Consistent with this structure, the cross section no longer depicts two separate wind speed maxima, but rather a single jet core with wind speeds in excess of 90 m s^{-1}. Particular attention is drawn to the 320-K and 325-K isentropes, highlighted in red, which are located at a significantly lower altitude beneath the jet core than at the prior times (Figs. 5b,d). This suggests that subsidence may have been responsible for the downward depression of these isentropes during the intervening 18 h and, therefore, potentially played a role in restructuring the tropopause into the characteristic superposed jet structure. The veracity of this inference is considered as part of the subsequent analysis.

3.2 Superposed Jet Formation

3.2.1. Subtropical Jet Evolution

Given that polar and subtropical jets are each associated with unique tropopause breaks, insight into the formation of a superposed jet can be garnered through a diagnosis of the movement of each individual tropopause break (i.e., jet axis), as they eventually become

vertically aligned. In this case, the existence of a subtropical jet was closely tied to the presence of remote tropical convection over portions of Central America and the eastern equatorial Pacific Ocean. One particularly insightful way to examine the effect that tropical convection can have on the subsequent evolution of the subtropical jet is through a consideration of the anomalous pressure depth of the isentropic layer that contains the subtropical jet. Particularly telling is the depth of that layer on the anticyclonic shear side of the jet, where positive perturbation depths correspond to excess mass, relative to a long term mean, residing in the layer. The perturbation pressure depths of various isentropic layers are calculated as the difference between instantaneous pressure depths and a 31-yr (1979-2009) average depth at that analysis time for each individual grid point, determined using NCEP's Climate Forecast System Reanalysis (CFSR) dataset (Saha et al. 2010). For the subtropical jet, we consider the pressure depth of the 340–355-K isentropic layer.

The outflow from tropical convection serves as one mechanism through which an isentropic layer can become anomalously inflated. Specifically, tropical convection often ingests boundary layer air with very high equivalent potential temperature (θ_e). Parcels embedded within convective updrafts are then exhausted at an isentropic level that roughly corresponds to this boundary layer θ_e . Often, such air is within the range of 340–355-K, coinciding with the isentropic layer that houses the subtropical jet. Furthermore, regions characterized by a strong horizontal gradient in perturbation pressure depth are associated with a perturbation geostrophic vertical shear, in accordance with the isentropic thermal wind relationship:

$$\frac{\partial \vec{V}_g'}{\partial \theta} = \frac{1}{\rho f \theta} \hat{k} \times \nabla p' \tag{2}$$

Consequently, a subtropical jet is typically positioned on the poleward edge of an area characterized by positive perturbation pressure depths in the 340–355-K isentropic layer.

Figure 6a demonstrates that at 0000 UTC 19 December, positive perturbation pressure depths in the 340–355-K isentropic layer were found over much of the Gulf of Mexico and Caribbean Sea on the anticyclonic shear side of the subtropical jet. Immediately upstream of the inflated isentropic layer were active areas of organized tropical convection over portions of the eastern equatorial Pacific Ocean and Central America (Fig. 6b), suggesting that convective outflow was a source of the excess mass found within the isentropic layer. Furthermore, the presence of weak, poleward-directed divergent winds at 200 hPa in the vicinity of the subtropical jet axis (red dashed line) induced a strip of negative PV advection within the 1–3-PVU channel along the subtropical tropopause break.[6] This negative PV advection suggested a poleward shift in the location of the subtropical jet axis, consistent with the observations made from Figs. 5a,c.

At 1800 UTC 19 December, perturbation pressure depths increased in both magnitude and areal coverage over a large portion of the central Caribbean and off the southeastern United States coast downstream of continued convection in the tropics (Figs. 6c,d). An inflation of the 340–355-K isentropic layer at this time is also apparent on the equatorward side of the subtropical jet within the cross section D-D' in Fig. 5d. Figure 6c indicates that weak, poleward-directed divergent winds continued to drive a well-defined strip of negative PV advection along the subtropical tropopause break, maintaining support for a poleward shift of the subtropical jet axis. Figure 7, however, depicts the total PV advection at 200 hPa accomplished by the full wind at this time, which indicates only localized regions of weak negative PV advection along the subtropical tropopause break over the Gulf of Mexico. This demonstrates that a large fraction of the negative PV advection accomplished by the divergent wind in Fig. 6c is mitigated by positive

[6] 200 hPa in this case, as well as the 2010 Nashville Flood, corresponds well to the level of maximum wind for the subtropical jet and cuts perpendicularly through the subtropical tropopause break (e.g., 2-PVU surface), allowing it to be a suitable level to assess the horizontal advection of the tropopause break by the divergent wind (e.g., Archambault et al. 2013; Archambault et al. 2015).

PV advection that must be associated with the non-divergent component of the flow in this location. Consequently, the role of the divergent wind appears to be slight, promoting only a slight poleward shift in the location of the subtropical jet. Figure 6e demonstrates that a subtle poleward shift in the location of the subtropical jet continued up until 1200 UTC 20 December when the polar and subtropical jets superposed. Furthermore, coincident with the superposed jet's increased wind speed at this time is a strengthened gradient in perturbation pressure depth immediately equatorward of the jet axis from the eastern Gulf of Mexico northeastward towards Bermuda.

The upper-tropospheric evolution in the hours preceding superposition strongly suggests that persistent remote tropical convection over the eastern equatorial Pacific Ocean and Central America was responsible for an inflation of the 340–355-K isentropic layer. An analysis of backward trajectories, using the NOAA/ARL HYSPLIT model (Draxler and Hess 1997; Draxler and Hess 1998; Draxler 1999; Draxler and Rolph 2015; Rolph 2015), for parcels originating at the center of the positive pressure perturbation at 1200 UTC 20 December (Fig. 8, see figure caption for more details on trajectory calculations) confirms this assertion. Specifically, Fig. 8 shows that roughly a fifth of the trajectories are characterized by rapid ascent around 0000 UTC 19 December in the vicinity of the tropical convection shown in Fig. 6b and warming to potential temperatures of 340–350-K. Upper-tropospheric southwesterly flow downstream of a low-latitude trough west of Mexico, which is identified by the cyclonic curvature of a few trajectories that initiate between 100-110^{o}W, subsequently acted to transport the convective outflow towards the Caribbean Sea in the 24-36 h prior to superposition, resulting in the positive perturbation pressure depths observed there. Forward trajectories (not shown) initiated at the center of the pressure perturbation at 1200 UTC 20 December show that parcels conserved their potential

temperature in the 72 h following jet superposition, as well, indicating little flow out of the 340–355-K isentropic layer. Consequently, there is strong evidence that the combination of both persistent tropical convection and the approach of a low-latitude trough contributed to the existence and maintenance of a subtropical jet over the Gulf of Mexico. First, by facilitating an inflation of the 340–355-K isentropic layer in the tropics and, secondly, by the subsequent translation of mass within that layer towards higher latitudes where it manifest itself as a positive pressure perturbation and was associated with an increase in westerly vertical shear on its poleward flank.

3.2.2. Polar Jet Evolution

Focusing attention on the evolution of the polar jet, and its interaction with the subtropical jet, Fig. 9a shows that the polar jet sat atop a region of enhanced baroclinicity that extended from northwestern Kansas southeastward into northern Mississippi at 0000 UTC 19 December. Furthermore, the geostrophic jet exit region was characterized by weak geostrophic cold air advection over southern Missouri and northern Arkansas. These circumstances support a poleward shift in the jet exit region's ageostrophic transverse circulation so as to position descent through the jet core (Fig. 4b). The solution for the Sawyer-Eliassen circulation within the cross section identified in Fig. 9a confirms this notion, depicting a region of subsidence centered squarely beneath the polar jet core (Fig. 10a). A comparison of Fig. 10a with the total GFS model vertical motion shown in Fig. 10b indicates a strong agreement between the model vertical motion and the distribution of subsidence associated with the transverse circulation. The subsidence driven by transverse circulation was specifically tied to the presence of dipole circulations, which consisted of a thermally direct (indirect) circulation to the south (north) of the jet core. This subsidence was not only responsible for strengthening the mid-tropospheric

405 temperature gradient via tilting, but also for supporting a downward protrusion of high PV air
406 associated with the development of the polar tropopause fold, as denoted by the strip of positive
407 PV advection driven by the circulation in the vicinity of the fold.

408 By 1800 UTC 19 December, the polar jet had propagated around the base of the polar
409 trough and assumed an orientation parallel to the axis of the subtropical jet over the southeastern
410 United States (Fig. 9b). Furthermore, geostrophic wind speeds associated with the polar jet
411 increased to greater than 60 m s^{-1}, in response to the intensified horizontal baroclinicity situated
412 beneath the jet. The magnitude of the geostrophic cold air advection also continued to strengthen
413 in the vicinity of both jets' entrance regions over northern Alabama, implying continued
414 subsidence in the vicinity of the jet cores.

415 The Sawyer-Eliassen circulation within the cross section D-D', drawn through the
416 entrance region of both the polar and subtropical jets at this time, is characterized by a strong
417 thermally direct circulation with subsidence confirmed directly on and beneath the subtropical
418 tropopause step[7] (Fig. 10c). It is likely that the strength of the circulation arises from its
419 proximity to the weakly stratified, tropical air mass located equatorward of the subtropical jet
420 (e.g., Lang and Martin 2013). The subsidence associated with the circulation also accounted for
421 the large majority of the positive PV advection diagnosed along the subtropical tropopause step
422 in Fig. 10c (not shown). Once again, the distribution of subsidence compared well with the
423 model vertical motion in Fig. 10d, which was also characterized by a maximum in subsidence
424 beneath the subtropical tropopause step that tilted equatorward with increasing elevation.
425 Consequently, it can be concluded that the diagnosed subsidence was favorably positioned to

[7] Cross sections along the entire length of the polar and subtropical jets at this time are consistent with the result shown in Fig. 10c.

advect high PV air downward and to lower the altitude of the subtropical tropopause step with time.

From another perspective, it is apparent that the 320-K and 325-K isentropes were situated within the horizontal baroclinicity that sat beneath the subtropical jet. The presence of a mid-tropospheric maximum in subsidence through the polar jet core, as indicated in Fig. 10c, implies that the 320-K isentrope was advected downward on the poleward side of the subtropical jet at a more rapid rate than the 325-K isentrope, reducing the horizontal baroclinicity beneath the subtropical jet. At the same time, the subsidence acted to incorporate these same isentropes into a strengthening region of baroclinicity beneath the polar jet core (Fig. 5f). Consequently, the subsidence associated with the Sawyer-Eliassen circulation promoted an intensification of the baroclinicity directly beneath the polar jet core at the expense of the subtropical jet's baroclinicity and, subsequently, the production of one consolidated region of intense horizontal temperature contrast that is characteristic of a superposed jet.

Also of note is the potential role that the upper-level branch of the transverse circulation may have played in horizontally displacing the subtropical tropopause break. Figure 10c indicates a region of negative PV advection that was centered squarely along the subtropical tropopause break and that was primarily attributable to the upper-level branch of the circulation (not shown). The magnitude of this negative PV advection also compares well with the negative PV advection by the full divergent wind at 200 hPa in Fig. 6c. However, given that the total horizontal PV advection along the subtropical tropopause break was found to be small (Fig. 7), it can be concluded that the influence of the upper-level branch of the circulation on restructuring the tropopause was relatively minimal compared to the circulation's subsiding branch.

By 1200 UTC 20 December, the polar tropopause break became vertically aligned with the subtropical tropopause break, producing the vertical PV wall shown in Fig. 5f and a superposed jet from central Georgia northeastward to eastern North Carolina (Fig. 9c). Wind speeds in the core of the superposed jet increased as well, consistent with the consolidation of baroclinicity beneath the superposed jet.

3.2.3 Synthesis

The preceding analysis of this case is summarized in the conceptual diagram shown in Fig. 11, which highlights the importance of internal jet dynamics for facilitating a vertical superposition of the polar and subtropical jets. While remote convection over Central America and the equatorial Pacific Ocean was essential for strengthening and establishing the subtropical jet over the Gulf of Mexico, the upper-tropospheric divergent wind only promoted a slight poleward shift in the location of the subtropical jet axis in that location. Ageostrophic transverse circulations, on the other hand, were crucial in their ability to restructure the tropopause into the two-step structure characteristic of a superposition. Specifically, the subsiding branches of these circulations were not only favorably positioned to support the production of a polar tropopause fold, but also to drive a downward protrusion of high PV air that was centered squarely on and beneath the subtropical tropopause step. Consequently, this subsidence, which was present throughout the 18 h period prior to superposition (not shown), was found to lower the tropopause height between the polar and subtropical jets and to consolidate the baroclinicity associated with each jet into a single zone of horizontal temperature contrast.

4. Jet Evolution during the 1-3 May 2010 Nashville Flood

4.1 Synoptic Overview

As described by WM14, the 1–3 May 2010 Nashville Flood was an historic two-day event in which two consecutive mesoscale convective systems (MCSs) were responsible for rainfall accumulations in excess of 180 mm (7 in.) across a large portion of Tennessee, southern Kentucky, and northern Mississippi (Moore et al. 2012, their Fig. 1). Moore et al. (2012) and Durkee et al. (2012) provide excellent overviews of both the meso- and synoptic-scale processes responsible for the production of precipitation in this case and the reader is referred to those works for any additional information. As with the December 2009 case, here we present an abbreviated synoptic overview that focuses solely on the jet evolution in the upper troposphere during the 24 h period of 0000 UTC 1 May 2010 – 0000 UTC 2 May 2010 across the contiguous United States.

Figure 12a depicts a high amplitude flow pattern in place over a large portion of North America at 0000 UTC 1 May, with a deep, positively tilted trough over the western United States and a strong ridge over the east. A polar jet was identified downstream of the trough axis and extended from Baja California northeastward into the Central Plains, while a subtropical jet, which was of comparable strength to the polar jet, stretched from northern Mexico eastward along the Gulf Coast. Note that at this time, even though the two jets are in close proximity to one another, they are not superposed. A cross section through the two separate jet cores (Fig. 12b) confirms this diagnosis and depicts a clear, three-step tropopause structure with each tropopause break associated with a distinct wind speed maximum.

At 1200 UTC 1 May, a broad area of precipitation situated over much of the Ohio River Valley helped to further build the extensive ridge that was in place over a large portion of the

494 eastern United States via a diabatic erosion of upper-tropospheric PV. This is best illustrated by a
495 substantial poleward retreat in the location of the 2-PVU contour at 200 hPa over the eastern
496 United States in Fig. 15. Consequently, in response to the strengthened ridge, the axis of the
497 subtropical jet shifted noticeably poleward and westward, bringing it closer to the polar jet (Fig.
498 12c). A cross section through the two jet structures at this time illustrates that a three-step
499 tropopause structure remained intact, while clearly showing the movement of the subtropical jet
500 towards the northwest and a wind speed increase in both jets (Fig. 12d).
501 At 0000 UTC 2 May, the polar and subtropical jets became superposed over portions of
502 west Texas and southwestern Oklahoma, as the axis of the subtropical jet continued to migrate
503 towards the northwest and the western trough shifted slowly eastward (Fig. 12e). A cross section
504 through the superposed portion of the jet (Fig. 12f) shows both the appearance of a slight
505 equatorward shift in the location of the polar tropopause break within the plane of the cross
506 section and the continued northwestward migration of the subtropical tropopause break, which
507 combined to produce the two-step tropopause structure and vertical PV wall characteristic of a
508 superposition. Further note that the two wind speed maxima are now consolidated into a single
509 jet core that featured wind speeds greater than 70 m s^{-1} in response to the increased horizontal
510 baroclinicity in the upper troposphere and lower stratosphere that accompanied the superposition
511 (Fig. 12f).
512 *4.2 Superposed Jet Formation*
513 4.2.1. Polar Jet Evolution
514 At 0000 UTC 1 May, the polar jet sat atop a rather extensive and continuous area of mid-
515 tropospheric baroclinicity that stretched from just off the coast of southern California into
516 northern Minnesota, as indicated by the 400 hPa temperature analysis in Fig. 13a. Furthermore,

517 the entrance region of the polar jet was characterized by an area of geostrophic cold air advection
518 centered squarely in the base of the western trough. This circumstance promotes subsidence
519 beneath the jet core (Shapiro 1982) by shifting the thermally direct circulation in the entrance
520 region towards the anticyclonic shear side of the jet (Fig. 4b).

521 The Sawyer-Eliassen circulation within the cross section identified in Fig. 13a illustrates
522 the presence of subsidence directly beneath the polar jet core and in the vicinity of the polar
523 tropopause fold (Fig. 14a). As for the circulations diagnosed in the previous case, the spatial
524 distribution of the subsidence associated with the transverse circulation in Fig. 14a matches well
525 with the distribution of model vertical motion shown in Fig. 14b. However, it is notable that the
526 subsidence in Fig. 14a is substantially weaker in magnitude and more spatially confined than its
527 model vertical motion counterpart. Nevertheless, the diagnosed subsidence, once again, promotes
528 a downward protrusion of high PV air into the middle troposphere, as denoted by the positive PV
529 advection situated in the polar tropopause fold in Fig. 14a, while simultaneously acting to
530 increase the horizontal baroclinicity beneath the jet via tilting. Subsequently, regions of strong
531 mid-tropospheric baroclinicity in Fig. 13 correspond roughly to the location of the polar
532 tropopause fold. It is also likely that the strong curvature associated with the western trough
533 further enhanced the total subsidence observed in the jet entrance region beyond that estimated
534 by the transverse circulation given the differences between Figs. 14a,b (see the maximum in 200
535 hPa velocity potential immediately upstream of the trough in Fig. 15 that suggests subsidence in
536 that location). Consequently, it is conceivable that flow curvature, in addition to the diagnosed
537 transverse circulation, acted to accentuate the development of the polar tropopause fold and to
538 strengthen the polar jet in this location.

539 At 1200 UTC 1 May, the axis of the polar jet became fractured near the United
540 States/Mexico border (Fig. 13b), partially due to the influence of ongoing convection over the
541 southern Mississippi River Valley and an associated region of negative PV advection along the
542 polar tropopause break driven by the divergent wind (not shown). Additionally, locations in the
543 vicinity of the jet fracture were characterized by an environment favorable for large-scale ascent,
544 given the close proximity of the upstream trough (see the minimum in velocity potential located
545 immediately downstream of the trough in Fig. 15). This large-scale ascent, while not explicitly
546 shown here, was responsible for decreasing the horizontal temperature gradient in the middle
547 troposphere via tilting downstream of the Rio Grande. Further upstream, in the base of the
548 trough, geostrophic jet wind speeds increased from the previous time in response to the
549 strengthened baroclinicity beneath the jet. Geostrophic cold air advection remained strong in the
550 base of the trough at this time as well, suggesting continued subsidence in the vicinity of the
551 polar jet core and the subsequent maintenance of the polar tropopause fold.
552 At 0000 UTC 2 May, the polar jet streak in the base of the trough was positioned slightly
553 downstream of its previous location, such that its most downstream edge overlapped with the
554 region of superposition identified in Fig. 12e over southwestern Oklahoma and west Texas (Fig.
555 13c). Furthermore, rather intense baroclinicity, which extended from the Southern Plains
556 upstream to Baja California, continued to characterize the polar jet stream. Recalling that this
557 area of baroclinicity was also associated with the development of a polar tropopause fold, it
558 becomes clear that the appearance of an equatorward displacement of the polar tropopause break
559 within Figs. 12d,f is simply the downstream propagation of an intense polar tropopause fold into
560 the area of superposition, as the trough slowly migrated eastward.
561

562 4.2.2. Subtropical Jet Evolution

563 As suggested, the evolution of the subtropical jet is closely tied to the persistent
564 convection present over portions of the southern Mississippi River Valley throughout the
565 duration of the flooding event. Recall that at 0000 UTC 1 May the subtropical jet was
566 characterized by a rather zonal orientation and was distinct from the polar jet (Fig. 12a).
567 Furthermore, Fig. 15a depicts an elongated minimum in velocity potential at 200 hPa
568 (approximately the level of maximum divergent outflow) centered over the Mississippi River
569 Valley, consistent with the presence of large-scale ascent in that location, and a maximum in
570 velocity potential immediately upstream of the trough over the western United States. The
571 juxtaposition of these two features resulted in the presence of easterly divergent winds over the
572 spine of the Rocky Mountains and northern Mexico. At this time, these divergent winds were
573 responsible for only a weak region of negative PV advection over northern Mexico along the
574 subtropical tropopause break, given its rather zonal orientation.

575 By 1200 UTC 1 May, it is apparent that latent heating from the ongoing convection over
576 the southern Mississippi River Valley (see Fig. 12c) had resulted in a substantial diabatic erosion
577 of upper-tropospheric PV in that location, as demonstrated by the poleward retreat of the 2-PVU
578 contour at 200 hPa (Fig. 15b). Consequently, the subtropical jet became characterized
579 predominantly by southwesterly flow and took on an orientation that was roughly parallel to the
580 polar jet. Divergent winds across northern Mexico also strengthened considerably over the
581 previous 12 h, largely due to the enhanced outflow from convection over portions of Tennessee
582 and southern Kentucky. The combination of these two factors resulted in a significantly more
583 favorable situation for the divergent wind to displace the subtropical tropopause break towards

584 the northwest, as indicated by the increase in negative PV advection along the subtropical
585 tropopause break.

586 The influence of the divergent wind is best analyzed in the context of Fig. 16, which
587 shows the total PV advection accomplished at 200 hPa at this time along the subtropical
588 tropopause break. From this analysis, it is evident that the divergent wind slows the eastward
589 translation of the subtropical tropopause break over northern Mexico, given the strip of positive
590 PV advection found in that location in Fig. 16. This mechanism, whereby the divergent wind
591 slows the eastward progression of a mid-latitude trough, is similar to that identified by
592 Archambault et al. (2015), among others, in cases of ET. Over Texas and Oklahoma, the
593 divergent and non-divergent wind fields appear to combine constructively to drive a region of
594 negative PV advection. Consequently, the northwestward shift in the position of the subtropical
595 jet axis over the Southern Plains is aided by the convective outflow and continued up until 0000
596 UTC 2 May, when the subtropical jet became vertically superposed with the polar jet over
597 portions of west Texas and southwestern Oklahoma (Fig. 15c).

598 4.2.3. Synthesis

599 In contrast to the December 2009 case, jet superposition in the May 2010 case was more
600 strongly dependent on the presence of convection over the southeastern United States. The
601 analysis, which is summarized in Fig. 17, demonstrates that the convection acted to substantially
602 restructure the tropopause via 1) the diabatic erosion of upper-tropospheric PV and, 2) advection
603 of the subtropical jet axis westward towards the polar jet via its associated divergent outflow.
604 This result aligns particularly well with existing evidence illustrating the role that tropopause-
605 level outflow can play in influencing the strength and location of a particular jet stream (e.g.,
606 Grams et al. 2011; Archambault et al. 2013; Grams et al. 2013; Archambault et al. 2015).

607 However, in contrast to the December 2009 case, ageostrophic transverse circulations played a
608 more indirect role in the production of a superposition during the 2010 Nashville Flood.
609 Specifically, persistent geostrophic cold air advection in the base of the western trough was
610 responsible for driving an area of subsidence in the vicinity of the polar jet core that facilitated
611 the development of a polar tropopause fold. This fold subsequently propagated downstream into
612 west Texas and southwestern Oklahoma by 0000 UTC 2 May where it undercut the retreating
613 subtropical tropopause break, thereby facilitating the development of the superposed jet
614 structure.

615 **5. Discussion**

616 Motivated by the identification of jet superpositions in several historic and recent high-
617 impact sensible weather events, this study examines the dynamical processes responsible for
618 producing a superposition during the 18–20 December 2009 Mid-Atlantic Blizzard and the 1–3
619 May 2010 Nashville Flood. The two cases selected highlight the fact that jet superpositions can
620 be associated with different types of high-impact weather events and can develop at different
621 times of year. Given that ageostrophic transverse jet circulations and convection both influence
622 the restructuring of the tropopause within single jet environments, the analysis focuses on the
623 role these same mechanisms play in reshaping the tropopause within the more complex double
624 jet environment.

625 Both cases were characterized by mid-tropospheric geostrophic cold air advection in
626 cyclonic shear along a portion of the polar jet at some point prior to superposition, indicating that
627 subsidence was positioned directly through and beneath the polar jet core. Consequently, the
628 descending motions were favorably positioned to facilitate downward advection of high PV air
629 from the stratosphere and contribute to the requisite restructuring of the tropopause that

630 characterizes a jet superposition. In the December 2009 case, this subsidence was specifically
631 positioned directly on and beneath the subtropical tropopause step and in the immediate vicinity
632 of both the polar and subtropical jets. Consequently, the subsidence played a primary role in the
633 production of a superposition by lowering the tropopause height in the region between the two
634 individual jets and by consolidating the baroclinicity associated with each jet into one single
635 zone of contrast. For comparison, only the jet entrance region of the polar jet was characterized
636 by subsidence during the May 2010 Flood. As a result, the subsidence in that case only fostered
637 the development of a polar tropopause fold, instead of working to directly assimilate the two jets
638 into a single structure.

639 The two cases examined as part of this study also demonstrate the different roles that
640 convection can play in facilitating a superposition. For instance, during the May 2010 Flood,
641 convection occurred in the immediate vicinity of the subtropical jet. This convection
642 subsequently acted to restructure the tropopause via material displacement and diabatic erosion
643 of upper-tropospheric PV and served as a primary mechanism supporting superposition in that
644 case. Conversely, the December 2009 case was associated with remote convection that occurred
645 in the tropics. This tropical convection was primarily responsible for substantially enhancing and
646 maintaining the strength of the subtropical jet by inflating the anticyclonic shear side of the
647 isentropic layer containing the jet. Together, these two cases demonstrate that the proximity of
648 convection to the jet structure can determine the nature of its influence on the jet. For example,
649 proximate convection can have a locally intense but temporally transient impact on the jet
650 structure through its divergent outflow and latent heat release. Alternatively, remote convection
651 can drive a slower acting, but persistent impact via the development of what might be termed

652 tropical tropopause anticyclones – the balanced response to upper-tropospheric mass deposition
653 on the anticyclonic shear side of the subtropical jet.

654 While both cases illustrate that internal jet dynamics and convection can play important
655 roles in the development of a superposition, it is clear that the individual importance of each
656 component to the process of jet superposition depends on the case being considered. For
657 instance, it appears that internal jet dynamics played a more prominent role during the December
658 2009 case, while convection was the dominant component during the May 2010 Flood. Given
659 that these are only two cases, a broader survey of jet superposition events over North America
660 may help 1) to pinpoint the variety of environmental characteristics that are most conducive for
661 the development of superpositions and 2) to determine whether or not that preferred environment
662 varies seasonally or geographically.

663 Another particularly useful way to investigate the physical processes involved in jet
664 superpositions is found by employing piecewise PV inversion techniques (e.g., Hoskins et al.
665 1985; Davis and Emanuel 1991). Specifically, as a product of ongoing work, we have developed
666 a scheme that isolates the individual PV anomalies associated with each jet structure by
667 considering the distribution of PV within isentropic layers characteristic to each jet. A prominent
668 outcome that emerges from an inversion of these PV anomalies, as well as those generated
669 diabatically from convection, is an ability to diagnose both the lateral and vertical interactions
670 between separate PV anomalies within a double jet environment and to assess the individual role
671 that each anomaly plays in restructuring the tropopause during the process of superposition.
672 Consequently, this analysis has the potential to better illuminate the importance of convection to
673 the process of superposition and to determine whether the three-dimensional circulation
674 associated with the polar or subtropical jet has a greater ability to restructure the tropopause.

675 Finally, persistent observation of these structures by the authors throughout the
676 development of this study has made clear that significant sensible weather is not tied to every jet
677 superposition event. Consequently, greater knowledge regarding the environmental differences
678 that exist between null cases and those associated with significant high-impact weather over
679 North America remains out standing. Ultimately, the ability to diagnose the formation of these
680 structures, and to understand the circumstances that permit them to contribute to the production
681 of high-impact weather at middle latitudes, could have important implications for short-term
682 weather prediction.
683
684 **Acknowledgments**
685 This work was supported by the National Science Foundation through grant NSF-
686 1265182. The authors are grateful for the comments from three anonymous reviewers, whose
687 input has greatly improved this manuscript.
688
689
690
691
692
693
694
695
696
697

698 **References**

699 Agusti-Panareda, A., C. D. Thorncroft, G. C. Craig, and S. L. Gray, 2004: The extratropical
700 transition of Hurricane Irene (1999): A potential-vorticity perspective. *Quart. J. Roy.*
701 *Meteor. Soc.*, **130,** 1047-1074.

702 Ahmadi-Givi, F., G. C. Graig, and R. S. Plant, 2004: The dynamics of a midlatitude cyclone with
703 very strong latent-heat release. *Quart. J. Roy. Meteor. Soc.*, **130,** 295-323.

704 Archambault, H. M., L. F. Bosart, D. Keyser, and J. M. Cordeira, 2013: A climatological
705 analysis of the extratropical flow response to recurving western North Pacific tropical
706 cyclones. *Mon. Wea. Rev.,* **141,** 2325-2346.

707 ———, D. Keyser, L. F. Bosart, C. A. Davis, and J. M. Cordeira, 2015: A composite perspective
708 of the extratropical flow response to recurving western North Pacific tropical cyclones.
709 *Mon. Wea. Rev.*, **143,** 1122-1141.

710 Bosart, L. F., G. J. Hakim, K. R. Tyle, M. A. Bedrick, W. E. Bracken, M. J. Dickinson, and D.
711 M. Schultz, 1996: Large-scale antecedent conditions associated with the 12-14 March
712 1993 cyclone ("Superstorm '93") over eastern North America. *Mon. Wea. Rev.*, **124,**
713 1865-1891.

714 Christenson, C. E., and J. E. Martin, 2012: The large-scale environment associated with the 25-
715 28 April 2011 severe weather outbreak. *16th NWA Severe Storms and Doppler Radar*
716 *Conference*, Des Moines, IA, National Weather Association, 31 March 2012.

717 ———, 2013: A synoptic-climatology of northern hemisphere polar and subtropical jet
718 superposition events. M.S. thesis, Department of Atmospheric and Oceanic Sciences,
719 University of Wisconsin-Madison, 62 pp.

720

721

722 Davis, C. A., and K. E. Emanuel, 1991: Potential vorticity diagnostics of cyclogenesis. *Mon.*
723 *Wea. Rev.*, **119,** 1929-1953.
724 Dean, D. B., and L. F. Bosart, 1996: Northern Hemisphere 500-hPa trough merger and fracture:
725 A climatology and case study. *Mon. Wea. Rev.,* **124,** 2644-2671.
726 Defant, F., 1959: On hydrodynamic instability caused by an approach of subtropical and
727 polarfront jet stream in northern latitudes before the onset of strong cyclogenesis. *The*
728 *Atmosphere and Sea in Motion,* New York, Rockefeller and Oxford University Presses,
729 305-325.
730 ———, and H. Taba, 1957: The threefold structure of the atmosphere and the characteristics of
731 the tropopause. *Tellus*, **9,** 259-275.
732 desJardins, M. L., K. F. Brill, and S. S. Schotz, 1991: Use of GEMPAK on UNIX workstations.
733 Preprints, *Seventh Int. Conf. on Interactive Information and Processing Systems for*
734 *Meteorology, Oceanography, and Hydrology,* New Orleans, LA, Amer. Meteor. Soc.,
735 449-453.
736 Draxler, R. R., 1999: HYSPLIT4 user's guide. NOAA Tech. Memo. ERL ARL-230, NOAA Air
737 Resources Laboratory, Silver Spring, MD.
738 ———, and G. D. Hess, 1997: Description of the HYSPLIT_4 modeling system. NOAA Tech.
739 Memo. ERL ARL-224, NOAA Air Resources Laboratory, Silver Spring, MD, 24 pp.
740 ———, and ———, 1998: An overview of the HYSPLIT_4 modeling system of trajectories,
741 dispersion, and deposition. *Aust. Meteor. Mag.,* **47,** 295-308.
742 ———, and G. D. Rolph, 2015: HYSPLIT (Hybrid Single-Particle Lagrangian Integrated
743 Trajectory) Model access via NOAA ARL READY Website

744 (http://ready.arl.noaa.gov/HYSPLIT.php). NOAA Air Resources Laboratory, Silver
745 Spring, MD.
746 Durkee, J. D., L. Campbell, K. Berry, D. Jordan, G. Goodrich, R. Mahmood, and S. Foster, 2012:
747 A synoptic perspective of the record 1-2 May 2010 mid-South heavy precipitation event.
748 *Bull. Amer. Meteor. Soc.*, **93,** 611-620.
749 Eichelberger, S. J., and D. L. Hartmann, 2007: Zonal jet structure and the leading mode of
750 variability. *J. Climate*, **20,** 5149-5163.
751 Eliassen, A., 1962: On the vertical circulation in frontal zones. *Goephys. Publ.*, **24,** 147-160.
752 Gaza, R. S., and L. F. Bosart, 1990: Trough merger characteristics over North America. *Wea.*
753 *Forecasting*, **5,** 314-331.
754 Grams, C. M., H. Wernli, M. Böttcher, J. Čampa, U. Corsmeier, S. C. Jones, J. H. Keller, C.-J.
755 Lenz, and L. Wiegand, 2011: The key role of diabatic processes in modifying the upper-
756 tropospheric wave guide: A North Atlantic case-study. *Quart. J. Roy. Meteor. Soc.*, **137,**
757 2174-2193.
758 ———, S. C. Jones, C. A. Davis, P. A. Harr, and M. Weissmann, 2013: The impact of Typhoon
759 Jangmi (2008) on the midlatitude flow. Part I: Upper-level ridgebuilding and
760 modification of the jet. *Quart. J. Roy. Meteor. Soc.,* **139,** 2148-2164.
761 Griffin, K. S., and L. F. Bosart, 2014: The extratropical transition of Tropical Cyclone Edisoana
762 (1990). *Mon. Wea. Rev.,* **142,** 2772-2793.
763 Hakim, G. J., L. F. Bosart, and D. Keyser, 1995: The Ohio Valley wave-merger cyclogenesis
764 event of 25-26 January 1978. Part I: Multiscale case study. *Mon. Wea. Rev.,* **123,** 2663-
765 2692.

766 ———, D. Keyser, and L. F. Bosart, 1996: The Ohio Valley wave merger cyclogenesis event of
767 25-26 January 1978. Part II: Diagnosis using quasigeostrophic potential vorticity
768 inversion. *Mon. Wea. Rev.*, **124,** 2176-2205.
769 Harnik, N., E. Galanti, O. Martius, and O. Adam, 2014: The anomalous merging of the African
770 and North Atlantic jet streams during Northern Hemisphere winter of 2010. *J. Climate*,
771 **27,** 7319-7334.
772 Hoskins, B. J., M. E. McIntyre, and A. W. Robertson, 1985: On the use and significance of
773 isentropic potential vorticity maps. *Quart. J. Roy. Meteor. Soc.*, **111,** 877-946.
774 ———, and P. Berrisford, 1988: A potential vorticity perspective of the storm of 15-16 October
775 1987. *Weather*, **43,** 122-129.
776 Keyser, D., and M. A. Shapiro, 1986: A review of the structure and dynamics of upper-level
777 frontal zones. *Mon. Wea. Rev.*, **114,** 452-499.
778 Koteswaram, P., 1953: An analysis of the high tropospheric wind circulation over India in
779 winter. *Indian J. Meteor. Geophys.*, **4,** 13-21.
780 ———, and S. Parthasarathy, 1954: The mean jet stream over Indian in the pre-monsoon and
781 post-monsoon seasons and vertical motions associated with subtropical jet streams.
782 *Indian J. Meteor. Geophys.*, **5,** 138-156.
783 Krishnamurti, T. N., 1961: The subtropical jet stream of winter. *J. Meteor.*, **18,** 172-191.
784 Lai, C.-C., and L. F. Bosart, 1988: A case study of trough merger in split westerly flow. *Mon.*
785 *Wea. Rev.,* **116,** 1838-1856.
786 Lang, A. A., and J. E. Martin, 2012: The structure and evolution of lower stratospheric frontal
787 zones. Part I: Examples in northwesterly and southwesterly flow. *Quart. J. Roy. Meteor.*
788 *Soc.*, **138,** 1350-1365.

———, and ———, 2013: The structure and evolution of lower stratospheric frontal zones. Part II: The influence of tropospheric convection on lower stratospheric frontal development. *Quart. J. Roy. Meteor. Soc.*, **139,** 1798-1809.

Lee, S., and H.-K. Kim, 2003: The dynamical relationship between subtropical and eddy-driven jets. *J. Atmos. Sci.*, **60,** 1490-1503.

Loewe, F. and V. Radok, 1950: A meridional aerological cross section in the southwest Pacific. *J. Meteor.*, **7,** 58-65.

Martin, J. E., 2014: Quasi-geostrophic diagnosis of the influence of vorticity advection on the development of upper level jet-front systems. *Quart. J. Roy. Meteor. Soc.*, in press.

Martius, O., C. Schwiertz, and H. C. Davies, 2010: Tropopause-level waveguides. *J. Atmos. Sci.,* **67,** 866-879.

McTaggart-Cowan, R., J. R. Gyakum, and M. K. Yau, 2001: Sensitivity testing of extratropical transitions using potential vorticity inversions to modify initial conditions: Hurricane Earl case study. *Mon. Wea. Rev.*, **129,** 1617-1636.

———, ———, and ———, 2004: The impact of tropical remnants on extratropical cyclogenesis: Case study of Hurricanes Danielle and Earl (1998). *Mon. Wea. Rev.*, **132,** 1933-1951.

———, L. F. Bosart, J. R. Gyakum, and E. H. Atallah, 2007: Hurricane Katrina (2005). Part II: Evolution and hemispheric impacts of a diabatically generated warm pool. *Mon. Wea. Rev.*, **135,** 3927-3949.

Mohri, K., 1953: On the fields of wind and temperature over Japan and adjacent waters during winter of 1950-1951. *Tellus*, **5,** 340-358.

811 Moore, B. J., P. J. Neiman, F. M. Ralph, and F. E. Barthold, 2012: Physical processes associated
812 with heavy flooding rainfall in Nashville, Tennessee, and vicinity during 1-2 May 2010:
813 The role of an atmospheric river and mesoscale convective systems. *Mon. Wea. Rev.*,
814 **140,** 358-378.
815 Morgan, M. C., and J. W. Nielsen-Gammon, 1998: Using tropopause maps to diagnose
816 midlatitude weather systems. *Mon. Wea. Rev.*, **126,** 241-265.
817 Namias, J., and P. F. Clapp, 1949: Confluence theory of the high tropospheric jet stream. *J.*
818 *Meteor.*, **6,** 330-336.
819 National Weather Service, cited 2014: December 18-19, 2009 winter storm. [Available online at
820 http://www4.ncsu.edu/~nwsfo/storage/cases/20091218/.]
821 Newton, C. W., 1954: Frontogenesis and frontolysis as a three-dimensional process. *J. Meteor.,*
822 **11,** 449-461.
823 O'Rourke, A. K., and G. K. Vallis, 2013: Jet interaction and the influence of a minimum phase
824 speed bound on the propagation of eddies. *J. Atmos. Sci.*, **70,** 2614-2628.
825 Palmén, E., and C. W. Newton, 1948: A study of the mean wind and temperature distribution in
826 the vicinity of the polar front in winter. *J. Meteor.*, **5,** 220-226.
827 ———, and ———, 1969: *Atmospheric Circulation Systems: Their Structure and Physical*
828 *Interpretation*. Academic Press, 603 pp.
829 Riehl, H., 1962: Jet streams of the atmosphere. Dept. of Atmospheric Science Tech. Rep. 32,
830 Colorado State University, Fort Collins, CO, 117 pp.
831 Rolph, G. D., 2015: Real-time Environmental Applications and Display sYstem (READY)
832 Website (http://ready.arl.noaa.gov). NOAA Air Resources Laboratory, Silver Spring,
833 MD.

834 Saha, S. and 51 co-authors, 2010: The NCEP Climate Forecast System Reanalysis. *Bull. Amer.*
835 *Meteor. Soc.*, **91,** 1015-1057.
836 Sawyer, J. S., 1956: The vertical circulation at meteorological fronts and its relation to
837 frontogenesis. *Proc. Roy. Soc. London,* **234A,** 346-362.
838 Shapiro, M. A., 1982: Mesoscale weather systems of the central United States. CIRES, 78 pp.
839 ———, and D. Keyser, 1990: Fronts, jet streams, and the tropopause. *Extratropical Cyclones:*
840 *The Erik Palmén Memorial Volume,* C. Newton and E. O. Holopainen, Eds., Amer.
841 Meteor. Soc., 167-191.
842 ———, H. Wernli, J.-W. Bao, J. Methven, X. Zou, J. Doyle, T. Holt, E. Donall-Grell, and P.
843 Neiman, 1999: A planetary-scale to mesoscale perspective of the life cycles of
844 extratropical cyclones: The bridge between theory and observations. *The Life Cycles of*
845 *Extratropical Cyclones*, M. Shapiro and S. Grønås, Eds., Amer. Meteor. Soc., 139-185.
846 Son, S.-W., and S. Lee, 2005: The response of westerly jets to thermal driving in a primitive
847 equation model. *J. Atmos. Sci.,* **62,** 3741-3757.
848 Strahl, J. L. S., and P. J. Smith, 2001: A diagnostic study of an explosively developing
849 extratropical cyclone and an associated 500-hPa trough merger. *Mon. Wea. Rev.,* **129,**
850 2310-2328.
851 Sutcliffe, R. C., 1947: A contribution to the problem of development. *Quart. J. Roy. Meteor.*
852 *Soc.*, **73,** 370-383.
853 ———, and J. K. Bannon, 1954: Seasonal changes in the upper-air conditions in the
854 Mediterranean Middle East area. *Proc. Int. Association of Meteorology*, Rome, Italy, Int.
855 Union of Geodesy and Geophysics. 322-334.

Winters, A. C., and J. E. Martin, 2014: The role of a polar/subtropical jet superposition in the May 2010 Nashville Flood. *Wea. Forecasting*, **29,** 954-974.

Yeh, T. C., 1950: The circulation of the high tropopause over China in the winter of 1945-46. *Tellus*, **2,** 173-183.

879 **Figure Captions**

880

881 FIG 1. Mean meridional cross section of potential temperature for 1 Jan 1956 with the polar,
882 subtropical, and tropical tropopauses labeled as indicated in the legend. The polar frontal layer is
883 shaded in gray (Winters and Martin 2014, their Fig. 2).

884

885 FIG 2. Northern Hemispheric map of tropopause height (hPa) at 0300 UTC 1 Jan 1956.
886 Tropopause breaks that correspond to the subtropical (STJ) and polar jet (POLJ) are labeled
887 accordingly. The area identified with a circle is a region characterized by a vertical superposition
888 of the polar and subtropical jets. Dark gray shading corresponds to the polar tropopause, white
889 shading to the subtropical tropopause, and light gray to the tropical tropopause (Winters and
890 Martin 2014, their Fig. 3)

891

892 FIG. 3. (a) The 300 hPa wind speeds (shaded every 10 m s^{-1} starting at 30 m s^{-1}) at 0000 UTC 27
893 Apr. 2010 depicting separate polar and subtropical jets. (b) Cross section A-A', in Fig. 3a,
894 through separate polar and subtropical jet cores with contours of 1-,2-, and 3-PVU (black); 4- ,5-
895 ,6- ,7- ,8-, and 9-PVU (light gray); potential temperature every 5 K (dashed gray); and wind
896 speed every 10 m s^{-1} beginning at 30 m s^{-1} (dark gray). The 315-330- and 340-355-K isentropic
897 layers, used to identify the locations of the jets, are shaded gray. The dark vertical lines
898 correspond to grid columns with the black dot confirming a positive identification of a polar or
899 subtropical jet. (c) As in (a), but for a superposed jet at 0000 UTC 24 Oct. 2010. (d) As in (b),
900 but for the cross section B-B', in Fig. 3c, with two positive identifications (black dots) within a
901 single grid column indicating a jet superposition (Winters and Martin 2014, their Fig. 4).

902

903 FIG. 4. Idealized configurations of jet circulations associated with a straight jet streak on an
904 isobaric surface in the upper troposphere. Geopotential height (thick solid lines), potential
905 temperature (dashed lines), geostrophic wind speed (fill pattern; with the jet speed maximum
906 represented by the J), and Sawyer-Eliassen vertical motions indicated by "up" and "down" for a
907 regime of (a) no geostrophic temperature advection, (b) upper-tropospheric geostrophic cold-air
908 advection, and (c) upper-tropospheric geostrophic warm-air advection along the jet axis (from
909 Lang and Martin 2012, their Fig. 3).

910

911 FIG. 5. [left column] 250 hPa wind speed is shaded with the gray fill pattern as indicated in the
912 legend, 250 hPa geopotential heights are contoured in red every 120 m, sea level pressure is
913 contoured with the dashed black lines every 4 hPa below 1000 hPa, the location of the sea-level
914 pressure minimum is identified with the red "L", and jet axes (identified with reference to the
915 WM14 jet identification scheme) are identified as specified in the legend for (a) 0000 UTC 19
916 December 2009, (c) 1800 UTC 19 December 2009, and (e) 1200 UTC 20 December 2009. [right
917 column] Cross sections, as identified in the plot immediately to its left, of wind speed shaded in
918 the blue fill pattern according to the legend, potential temperature contoured every 5 K (dashed
919 green lines), and contours of 1-,2-, and 3-PVU (black) at (b) 0000 UTC 19 December 2009, (d)
920 1800 UTC 19 December 2009, and (f) 1200 UTC 20 December 2009. The gray shaded isentropic
921 layers are those used to identify the jet axes using the identification scheme outlined in the text
922 and the 320-K and 325-K isentropes are highlighted with the dashed red lines in the cross
923 sections for reasons discussed in the text.

924

925 FIG. 6. [left column] 200 hPa geopotential height is contoured in red every 120 m, 200 hPa
926 geostrophic wind speed is shaded with the gray fill pattern according to the legend, positive
927 perturbation pressure depths within the 340-355-K isentropic layer are shaded in the green fill
928 pattern according to the legend, negative PV advection within the 1–3-PVU channel by the
929 divergent wind (arrows) is contoured in yellow every $2x10^{-5}$ PVU s^{-1}, and the subtropical jet axis
930 from Fig. 5 is identified with the thick, dashed red line for (a) 0000 UTC 19 December 2009, (c)
931 1800 UTC 19 December 2009, and (e) 1200 UTC 20 December 2009. [right column] Infrared
932 satellite imagery from University of Wisconsin – CIMSS for (b) 0000 UTC 19 December 2009,
933 (d) 1800 UTC 19 December 2009, and (f) 1200 UTC 20 December 2009. The yellow box
934 denotes the source region for the trajectories shown in Fig. 8.
935
936 FIG. 7. 200 hPa positive (negative) PV advection within the 1–3 PVU channel by the total wind
937 contoured in purple (green) every $2x10^{-5}$ PVU s^{-1} and the 2-PVU surface at 300 hPa (200 hPa)
938 contoured in blue (red), which corresponds to the location of the polar (subtropical) tropopause
939 break.
940
941 FIG. 8. 48 h backward trajectories initialized at 1200 UTC 20 December 2009 every 1^{o}
942 latitude/longitude within the yellow box (20^{o}N–25^{o}N; 80^{o}W–70^{o}W) shown in Fig. 6e.
943 Trajectories were initialized at 12000 m AGL within the NOAA/ARL HYSPLIT model and
944 projected backward using archived NCEP Global Data Assimilation System (GDAS) data and
945 model vertical motion. The GDAS data has a horizontal resolution of 1.0^{o} x1.0^{o}, is interpolated
946 from 23 sigma levels to the mandatory pressure levels, and has a temporal resolution of 3 h. The

947 bottom panel depicts the potential temperature of the trajectories throughout the duration of the
948 simulation.
949
950 FIG. 9. 250 hPa geostrophic wind speed is shaded with the gray fill pattern according to the
951 legend, 300 hPa geostrophic cold (warm) air advection is shaded in the blue (red) fill pattern
952 following the legend, 500 hPa potential temperature is contoured in red every 3 K, and sea level
953 pressure is contoured with the dashed black lines every 4 hPa below 1000 hPa for (a) 0000 UTC
954 19 December 2009, (b) 1800 UTC 19 December 2009, and (c) 1200 UTC 20 December 2009.
955 The polar (subtropical) jet axis is indicated by the thick, dashed blue (red) line, as in Fig. 5, the
956 yellow circle highlights the region of jet superposition, and the red "L" marks the location of the
957 sea level pressure minimum.
958
959 FIG. 10. (a,c) Cross sections, as indicated in Fig. 9, of Sawyer-Eliassen streamfunction every 300
960 m hPa s^{-1} with negative (positive) values contoured with dashed (solid) black lines, potential
961 temperature every 5 K contoured in red, positive omega associated with the Sawyer-Eliassen
962 circulation shaded in the purple fill pattern following the legend, geostrophic wind speeds shaded
963 with the gray fill pattern according to the legend, positive (negative) PV advection within the 1–
964 3-PVU channel by the Sawyer-Eliassen circulation contoured with the solid (dashed) yellow
965 lines every $2x10^{-5}$ PVU s^{-1}, and the 1.5-PVU surface identified by the bold blue line. The sense
966 of the circulation is depicted by the arrowheads plotted on the streamfunction contours. The 320
967 K and 325 K isentropes are bolded in (c) for reasons discussed in the text. (b,d) Wind speed, PV,
968 and potential temperature distributions are identical to those in (a,c) with subsidence from the
969 GFS analysis now shaded in the purple fill pattern.

970

971 FIG. 11. Conceptual diagram summarizing the development of a superposed jet during the 18–20
972 December 2009 Mid-Atlantic Blizzard. “TENN” corresponds to Tennessee and “GULF” denotes
973 the location of the Gulf Coast.

974

975 FIG. 12. Conventions are identical to Fig. 5 but for (a,b) 0000 UTC 1 May 2010, (c,d) 1200 UTC
976 1 May 2010, and (e,f) 0000 UTC 2 May 2010. The precipitation shield at 1200 UTC 1 May 2010
977 in (c) is denoted by the green shading and sea level pressure is now contoured every 4 hPa below
978 996 hPa in the left column.

979

980 FIG. 13. 300 hPa geostrophic wind speed is shaded in the gray fill pattern according to the
981 legend, 300 hPa geostrophic cold (warm) air advection is shaded in the blue (red) fill pattern
982 following the legend, and 400 hPa potential temperature is contoured in red every 3 K at (a) 0000
983 UTC 1 May 2010, (b) 1200 UTC 1 May 2010, and (c) 0000 UTC 2 May 2010. Polar jet axes
984 from Fig. 12 are indicated by the thick, blue dashed lines and the yellow circle highlights the
985 region of jet superposition.

986

987 FIG. 14. Conventions are identical to those in Fig. 10, but for the cross section shown in Fig.
988 13a.

989

990 FIG. 15. 200 hPa velocity potential is contoured every 3×10^6 m^2 s^{-1} with positive (negative)
991 values identified with solid (dashed) thick red lines, the 2-PVU contour at 300 hPa (200 hPa) is
992 identified with the thick blue (red) line, and negative PV advection within the 1–3-PVU channel

993 by the divergent wind (arrows) at 200 hPa is shaded in the green fill pattern following the legend
994 at (a) 0000 UTC 1 May 2010, (b) 1200 UTC 1 May 2010, and (c) 0000 UTC 2 May 2010.
995
996 FIG. 16. Conventions are identical to those in Fig. 7, but at 1200 UTC 1 May 2010.
997
998 FIG. 17. Conceptual diagram summarizing the development of a superposed jet during the 1–3
999 May 2010 Nashville Flood. “OKLA” corresponds to Oklahoma and “GULF” denotes the
1000 location of the Gulf Coast.
1001
1002
1003
1004
1005
1006
1007
1008
1009
1010
1011
1012
1013
1014
1015

Figures

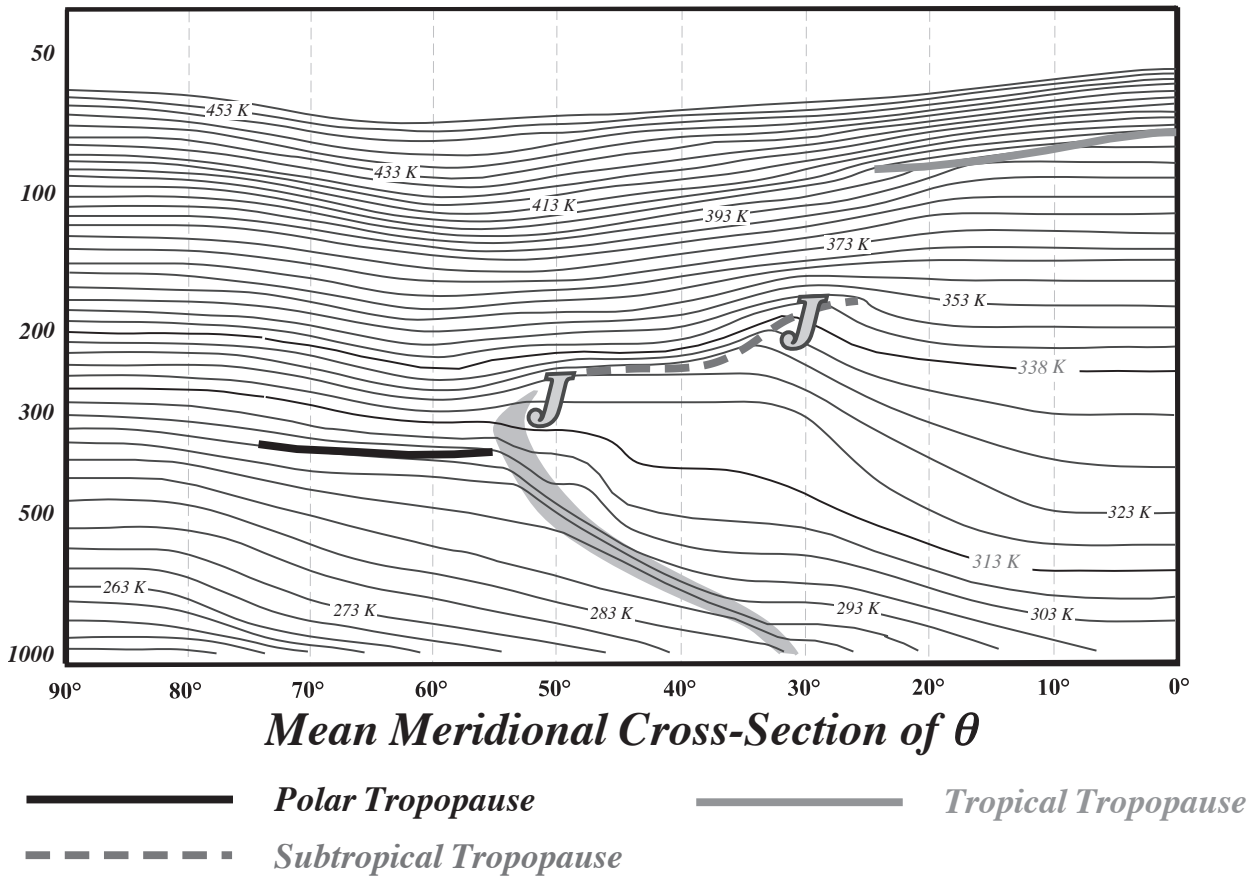

FIG 1. Mean meridional cross section of potential temperature for 1 Jan 1956 with the polar, subtropical, and tropical tropopauses labeled as indicated in the legend. The polar frontal layer is shaded in gray (Winters and Martin 2014, their Fig. 2).

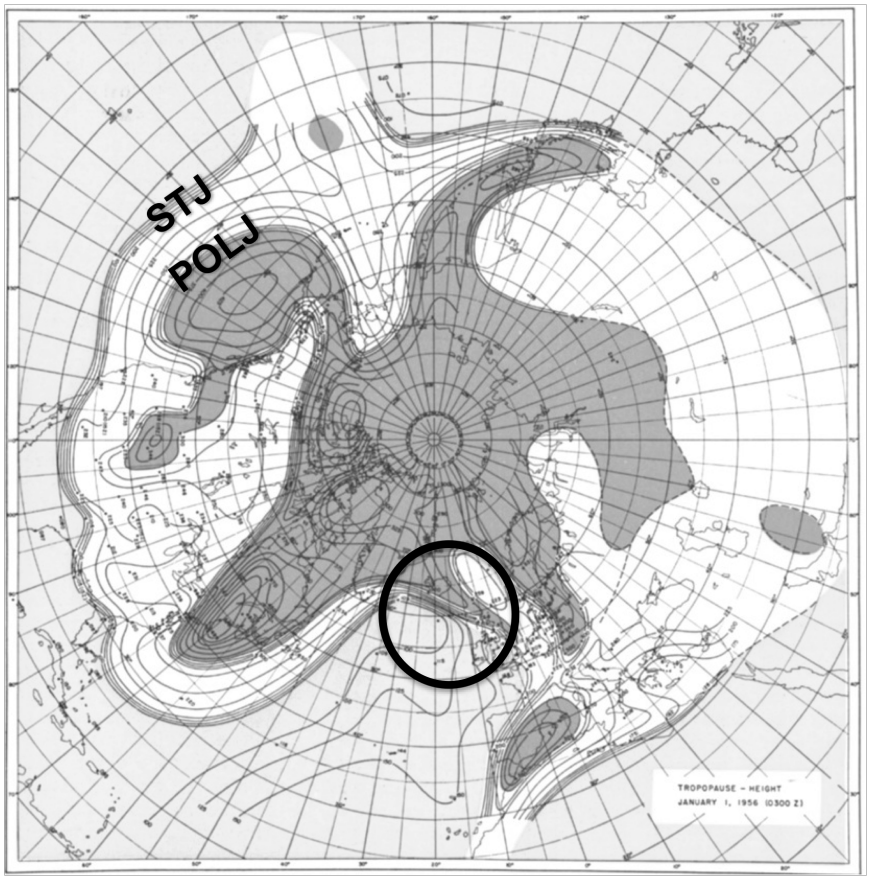

FIG 2. Northern Hemispheric map of tropopause height (hPa) at 0300 UTC 1 Jan 1956. Tropopause breaks that correspond to the subtropical (STJ) and polar jet (POLJ) are labeled accordingly. The area identified with a circle is a region characterized by a vertical superposition of the polar and subtropical jets. Dark gray shading corresponds to the polar tropopause, white shading to the subtropical tropopause, and light gray to the tropical tropopause (Winters and Martin 2014, their Fig. 3)

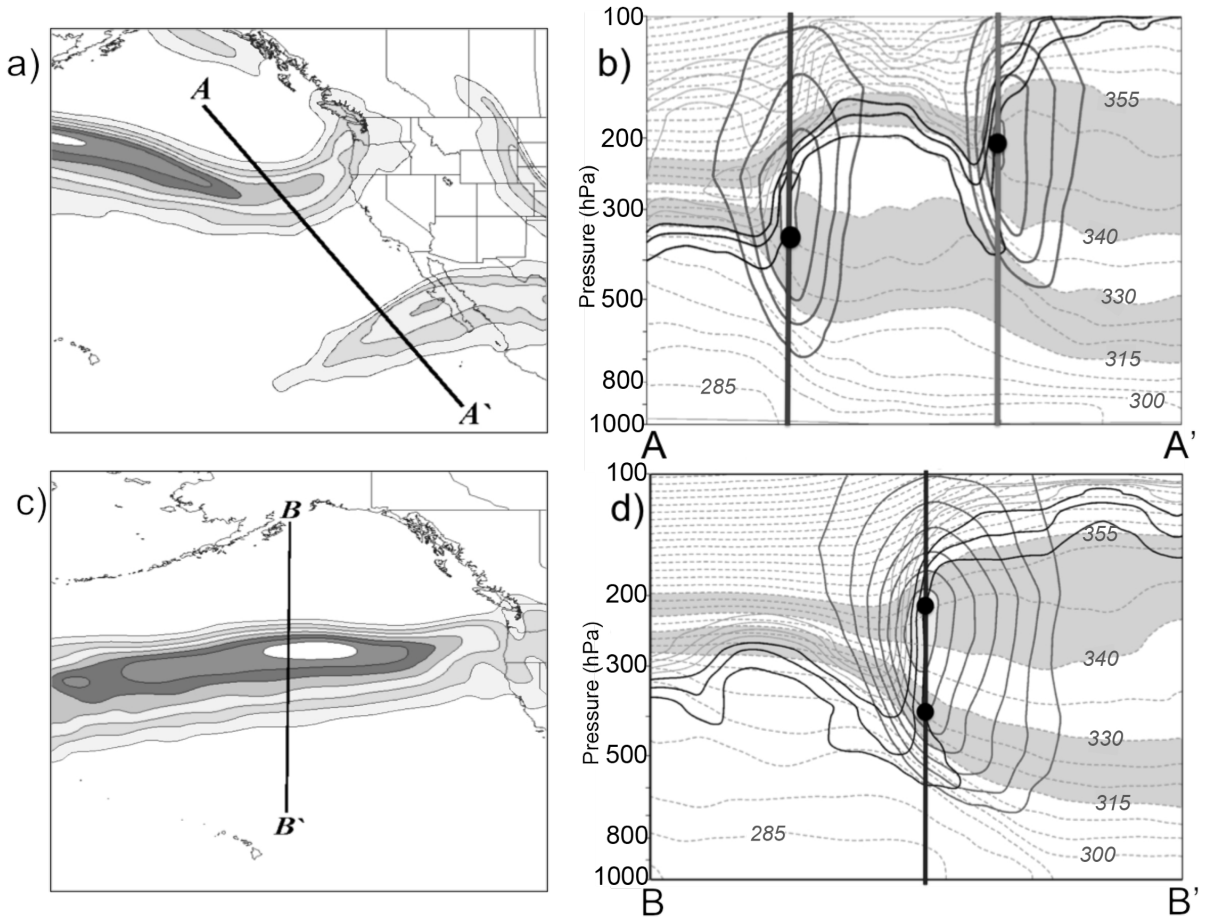

FIG. 3. (a) The 300 hPa wind speeds (shaded every 10 m s^{-1} starting at 30 m s^{-1}) at 0000 UTC 27 Apr. 2010 depicting separate polar and subtropical jets. (b) Cross section A-A', in Fig. 3a, through separate polar and subtropical jet cores with contours of 1-,2-, and 3-PVU (black); 4- ,5- ,6- ,7- ,8-, and 9-PVU (light gray); potential temperature every 5 K (dashed gray); and wind speed every 10 m s^{-1} beginning at 30 m s^{-1} (dark gray). The 315-330- and 340-355-K isentropic layers, used to identify the locations of the jets, are shaded gray. The dark vertical lines correspond to grid columns with the black dot confirming a positive identification of a polar or subtropical jet. (c) As in (a), but for a superposed jet at 0000 UTC 24 Oct. 2010. (d) As in (b), but for the cross section B-B', in Fig. 3c, with two positive identifications (black dots) within a single grid column indicating a jet superposition (Winters and Martin 2014, their Fig. 4).

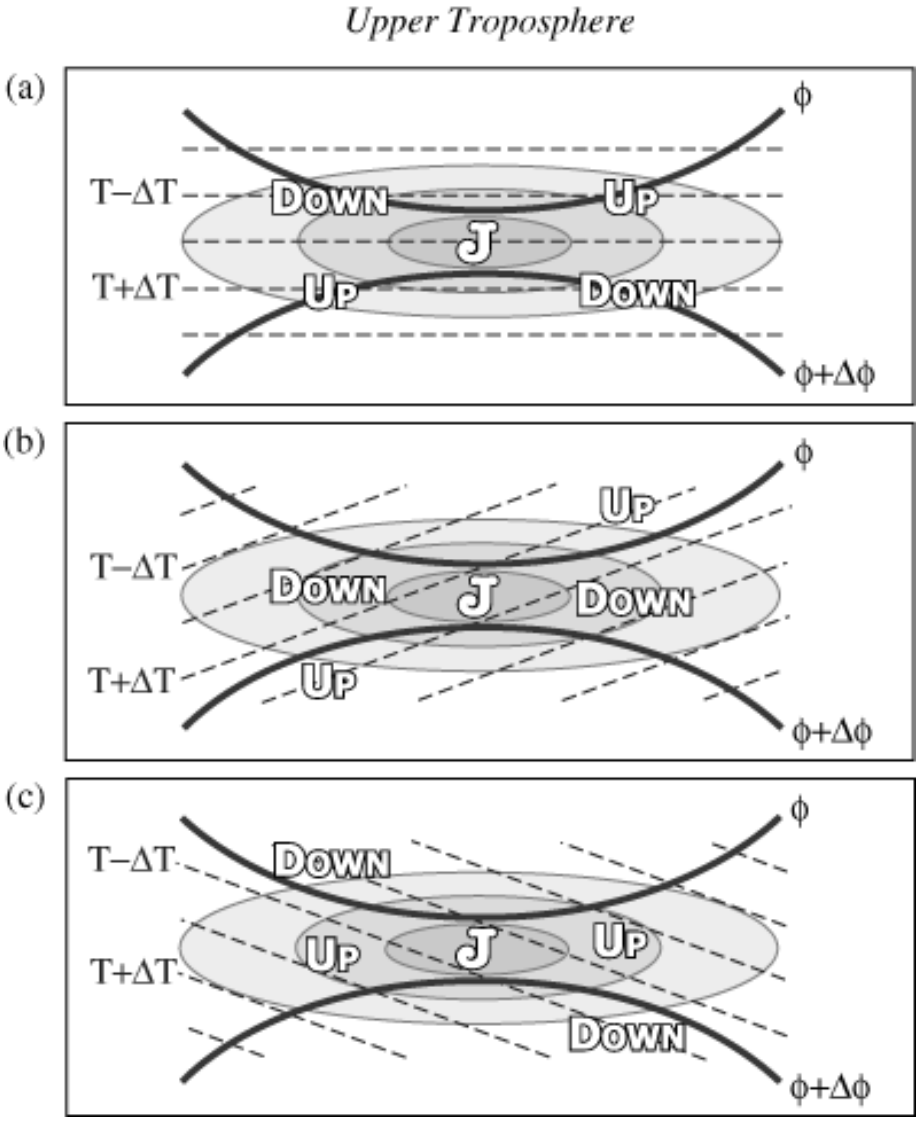

FIG. 4. Idealized configurations of jet circulations associated with a straight jet streak on an isobaric surface in the upper troposphere. Geopotential height (thick solid lines), potential temperature (dashed lines), geostrophic wind speed (fill pattern; with the jet speed maximum represented by the J), and Sawyer-Eliassen vertical motions indicated by "up" and "down" for a regime of (a) no geostrophic temperature advection, (b) upper-tropospheric geostrophic cold-air advection, and (c) upper-tropospheric geostrophic warm-air advection along the jet axis (from Lang and Martin 2012, their Fig. 3).

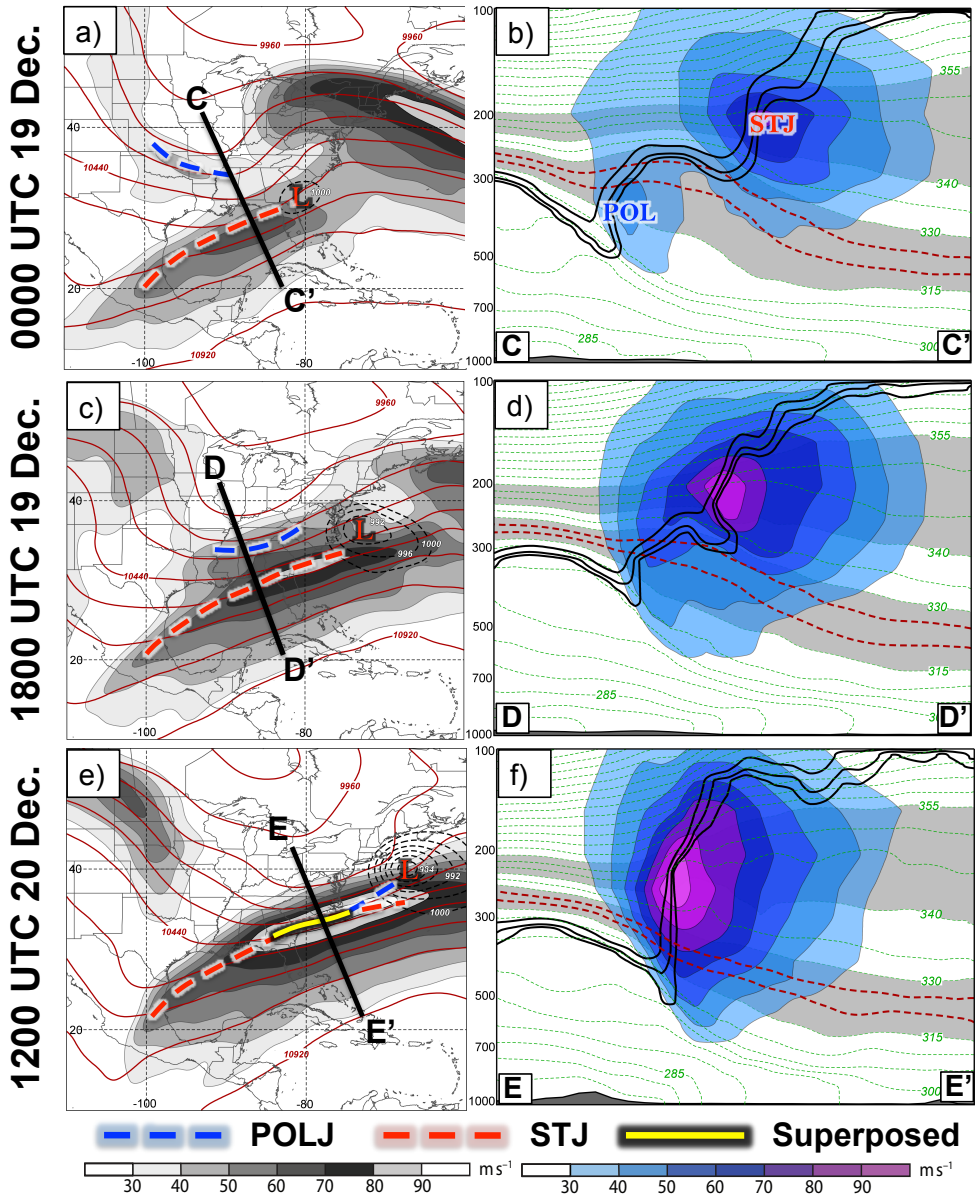

FIG. 5. [left column] 250 hPa wind speed is shaded with the gray fill pattern as indicated in the legend, 250 hPa geopotential heights are contoured in red every 120 m, sea level pressure is contoured with the dashed black lines every 4 hPa below 1000 hPa, the location of the sea-level pressure minimum is identified with the red "L", and jet axes (identified with reference to the WM14 jet identification scheme) are identified as specified in the legend for (a) 0000 UTC 19 December 2009, (c) 1800 UTC 19 December 2009, and (e) 1200 UTC 20 December 2009. [right column] Cross sections, as identified in the plot immediately to its left, of wind speed shaded in the blue fill pattern according to the legend, potential temperature contoured every 5 K (dashed green lines), and contours of 1-,2-, and 3-PVU (black) at (b) 0000 UTC 19 December 2009, (d) 1800 UTC 19 December 2009, and (f) 1200 UTC 20 December 2009. The gray shaded isentropic layers are those used to identify the jet axes using the identification scheme outlined in the text and the 320-K and 325-K isentropes are highlighted with the dashed red lines in the cross sections for reasons discussed in the text.

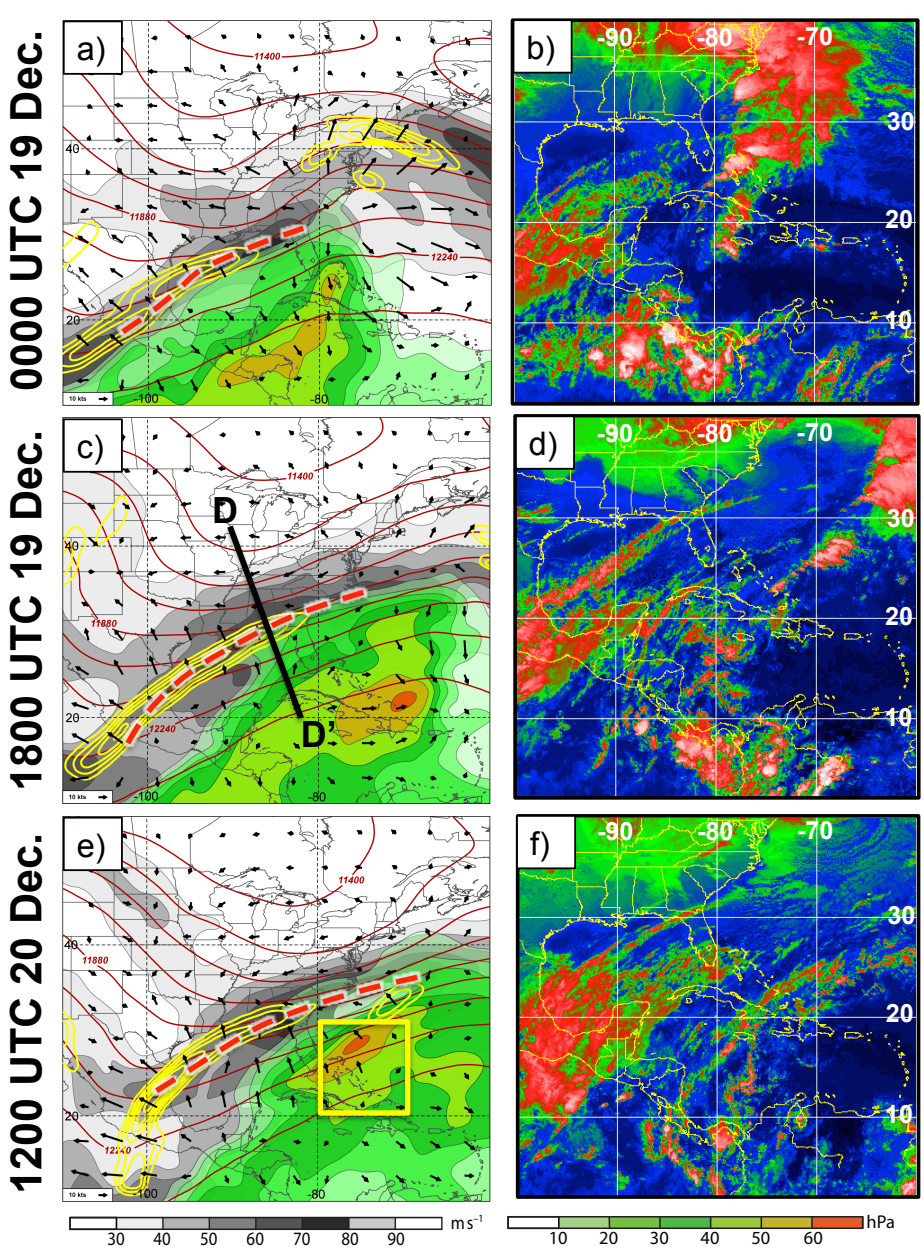

FIG. 6. [left column] 200 hPa geopotential height is contoured in red every 120 m, 200 hPa geostrophic wind speed is shaded with the gray fill pattern according to the legend, positive perturbation pressure depths within the 340-355-K isentropic layer are shaded in the green fill pattern according to the legend, negative PV advection within the 1–3-PVU channel by the divergent wind (arrows) is contoured in yellow every 2×10^{-5} PVU s^{-1}, and the subtropical jet axis from Fig. 5 is identified with the thick, dashed red line for (a) 0000 UTC 19 December 2009, (c) 1800 UTC 19 December 2009, and (e) 1200 UTC 20 December 2009. [right column] Infrared satellite imagery from University of Wisconsin – CIMSS for (b) 0000 UTC 19 December 2009, (d) 1800 UTC 19 December 2009, and (f) 1200 UTC 20 December 2009. The yellow box denotes the source region for the trajectories shown in Fig. 8.

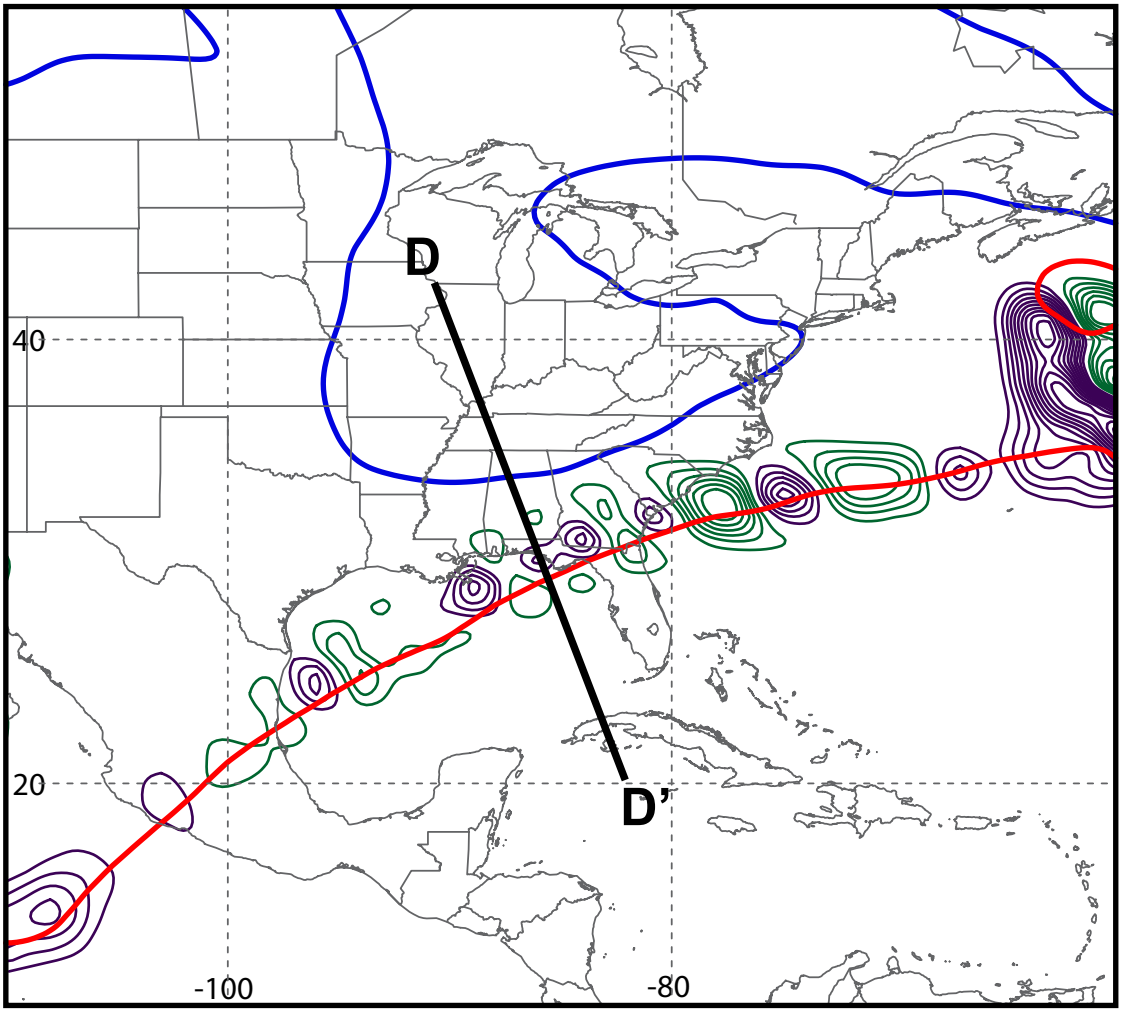

FIG. 7. 200 hPa positive (negative) PV advection within the 1–3 PVU channel by the total wind contoured in purple (green) every $2x10^{-5}$ PVU s^{-1} and the 2-PVU surface at 300 hPa (200 hPa) contoured in blue (red), which corresponds to the location of the polar (subtropical) tropopause break.

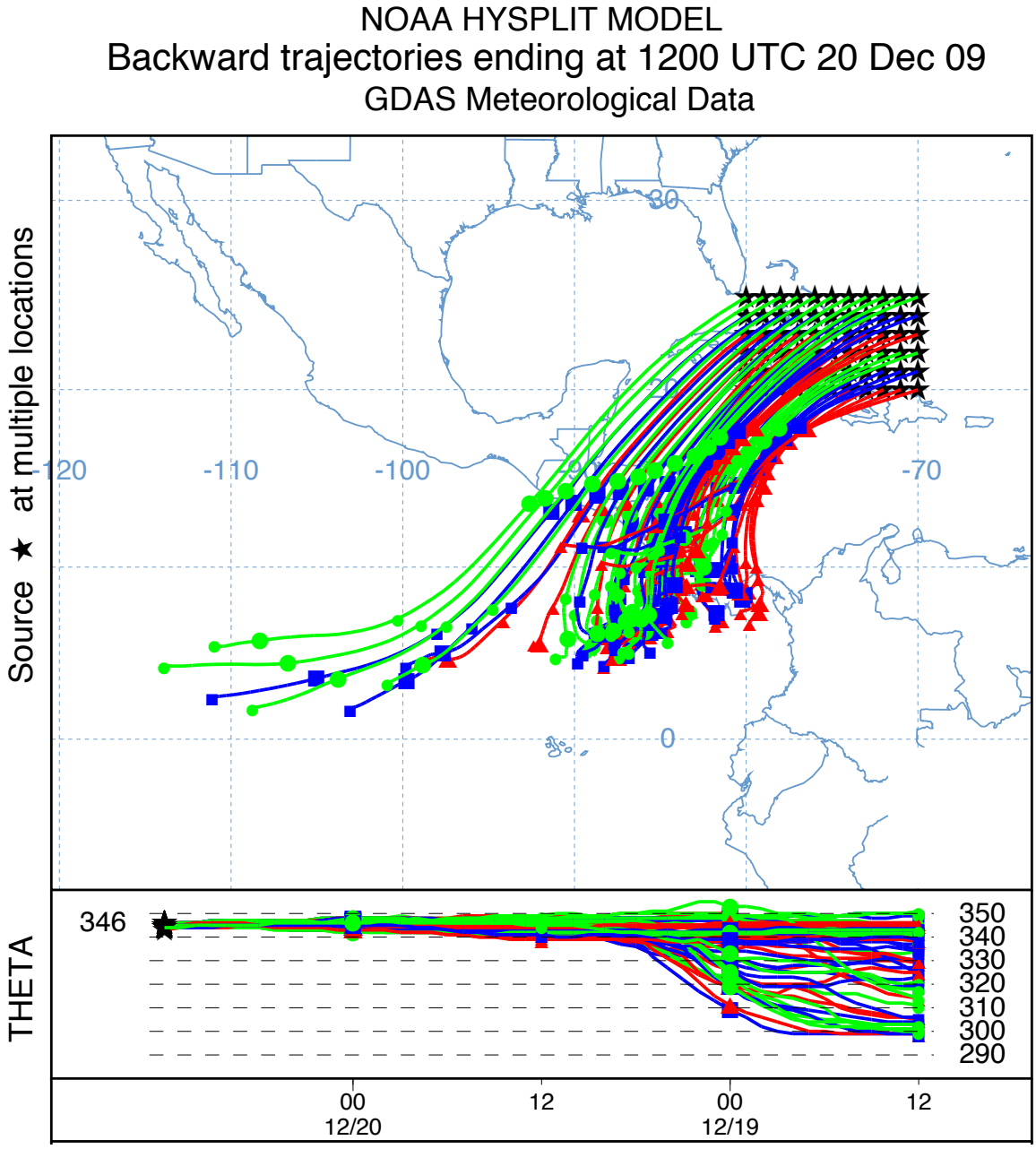

FIG. 8. 48 h backward trajectories initialized at 1200 UTC 20 December 2009 every 1° latitude/longitude within the yellow box (20°N–25°N; 80°W–70°W) shown in Fig. 6e. Trajectories were initialized at 12000 m AGL within the NOAA/ARL HYSPLIT model and projected backward using archived NCEP Global Data Assimilation System (GDAS) data and model vertical motion. The GDAS data has a horizontal resolution of 1.0° x1.0°, is interpolated from 23 sigma levels to the mandatory pressure levels, and has a temporal resolution of 3 h. The bottom panel depicts the potential temperature of the trajectories throughout the duration of the simulation.

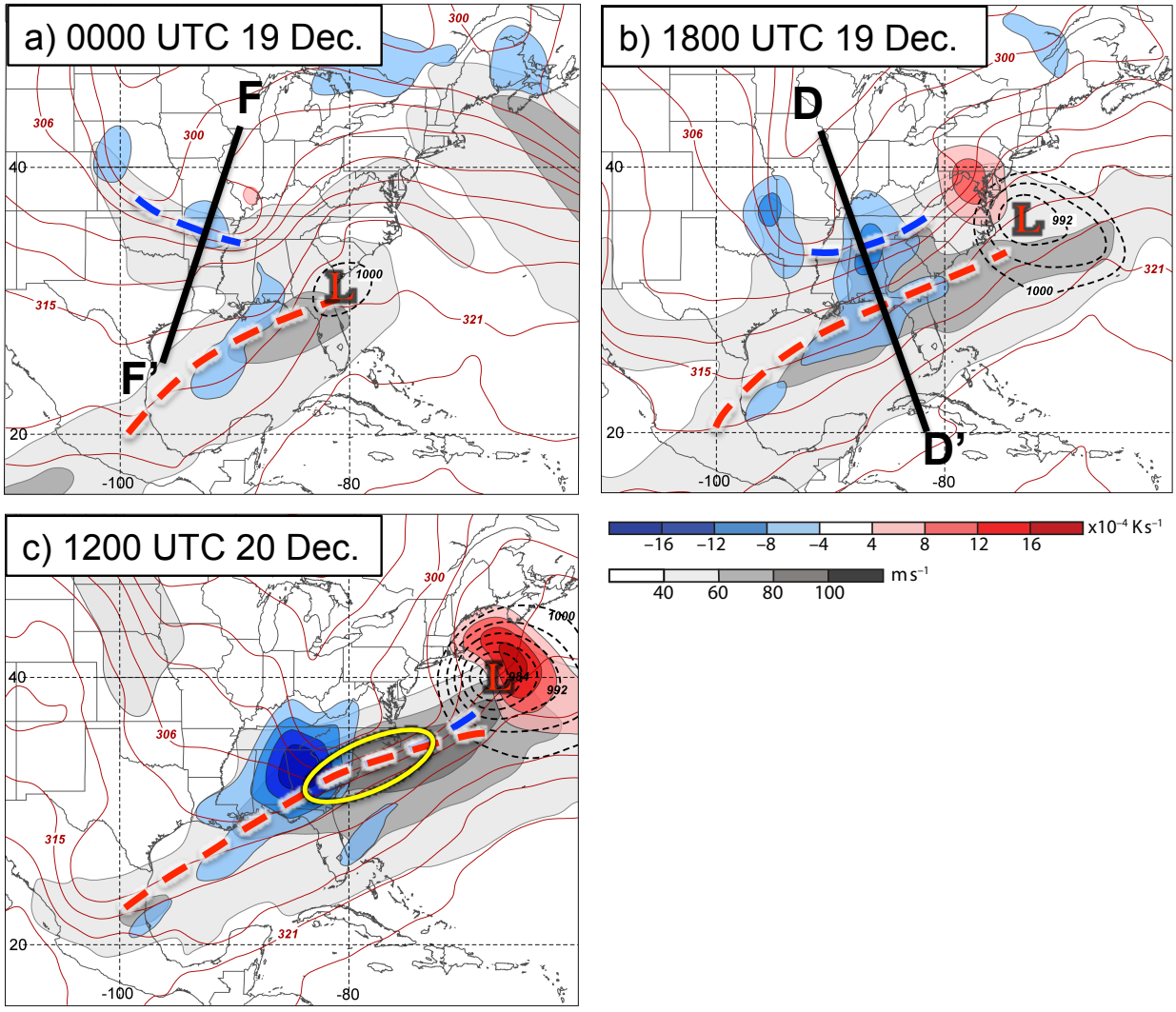

FIG. 9. 250 hPa geostrophic wind speed is shaded with the gray fill pattern according to the legend, 300 hPa geostrophic cold (warm) air advection is shaded in the blue (red) fill pattern following the legend, 500 hPa potential temperature is contoured in red every 3 K, and sea level pressure is contoured with the dashed black lines every 4 hPa below 1000 hPa for (a) 0000 UTC 19 December 2009, (b) 1800 UTC 19 December 2009, and (c) 1200 UTC 20 December 2009. The polar (subtropical) jet axis is indicated by the thick, dashed blue (red) line, as in Fig. 5, the yellow circle highlights the region of jet superposition, and the red "L" marks the location of the sea level pressure minimum.

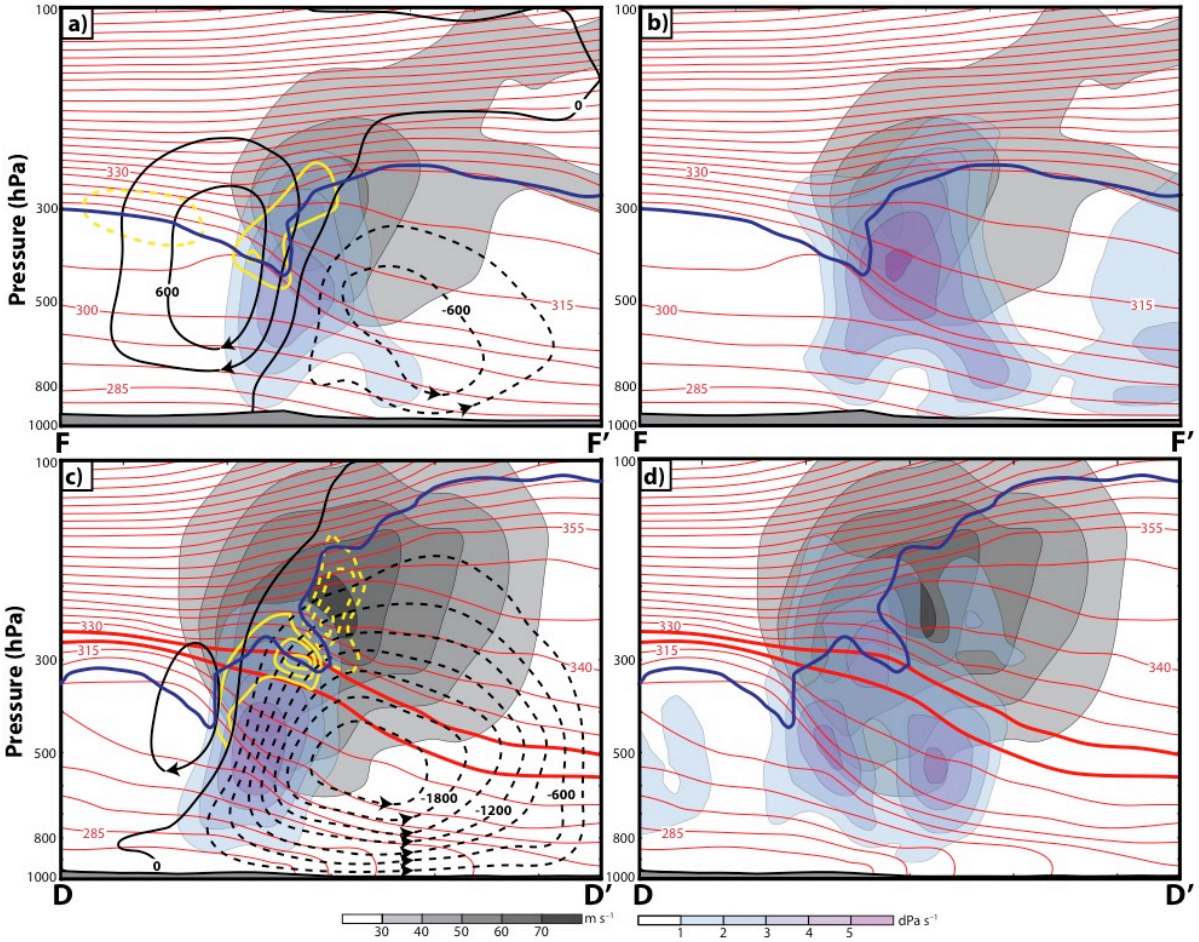

FIG. 10. (a,c) Cross sections, as indicated in Fig. 9, of Sawyer-Eliassen streamfunction every 300 m hPa s^{-1} with negative (positive) values contoured with dashed (solid) black lines, potential temperature every 5 K contoured in red, positive omega associated with the Sawyer-Eliassen circulation shaded in the purple fill pattern following the legend, geostrophic wind speeds shaded with the gray fill pattern according to the legend, positive (negative) PV advection within the 1–3-PVU channel by the Sawyer-Eliassen circulation contoured with the solid (dashed) yellow lines every $2x10^{-5}$ PVU s^{-1}, and the 1.5-PVU surface identified by the bold blue line. The sense of the circulation is depicted by the arrowheads plotted on the streamfunction contours. The 320 K and 325 K isentropes are bolded in (c) for reasons discussed in the text. (b,d) Wind speed, PV, and potential temperature distributions are identical to those in (a,c) with subsidence from the GFS analysis now shaded in the purple fill pattern.

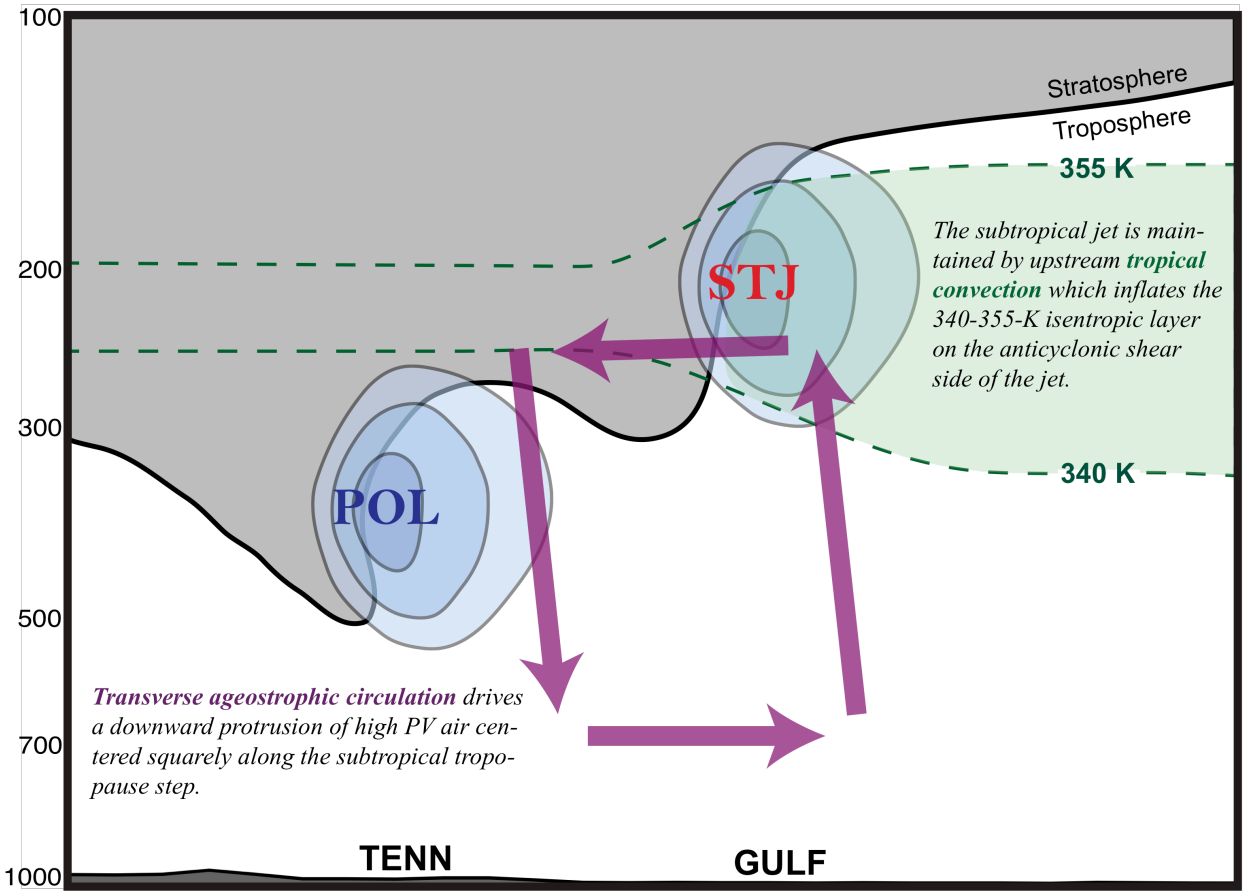

FIG. 11. Conceptual diagram summarizing the development of a superposed jet during the 18–20 December 2009 Mid-Atlantic Blizzard. "TENN" corresponds to Tennessee and "GULF" denotes the location of the Gulf Coast.

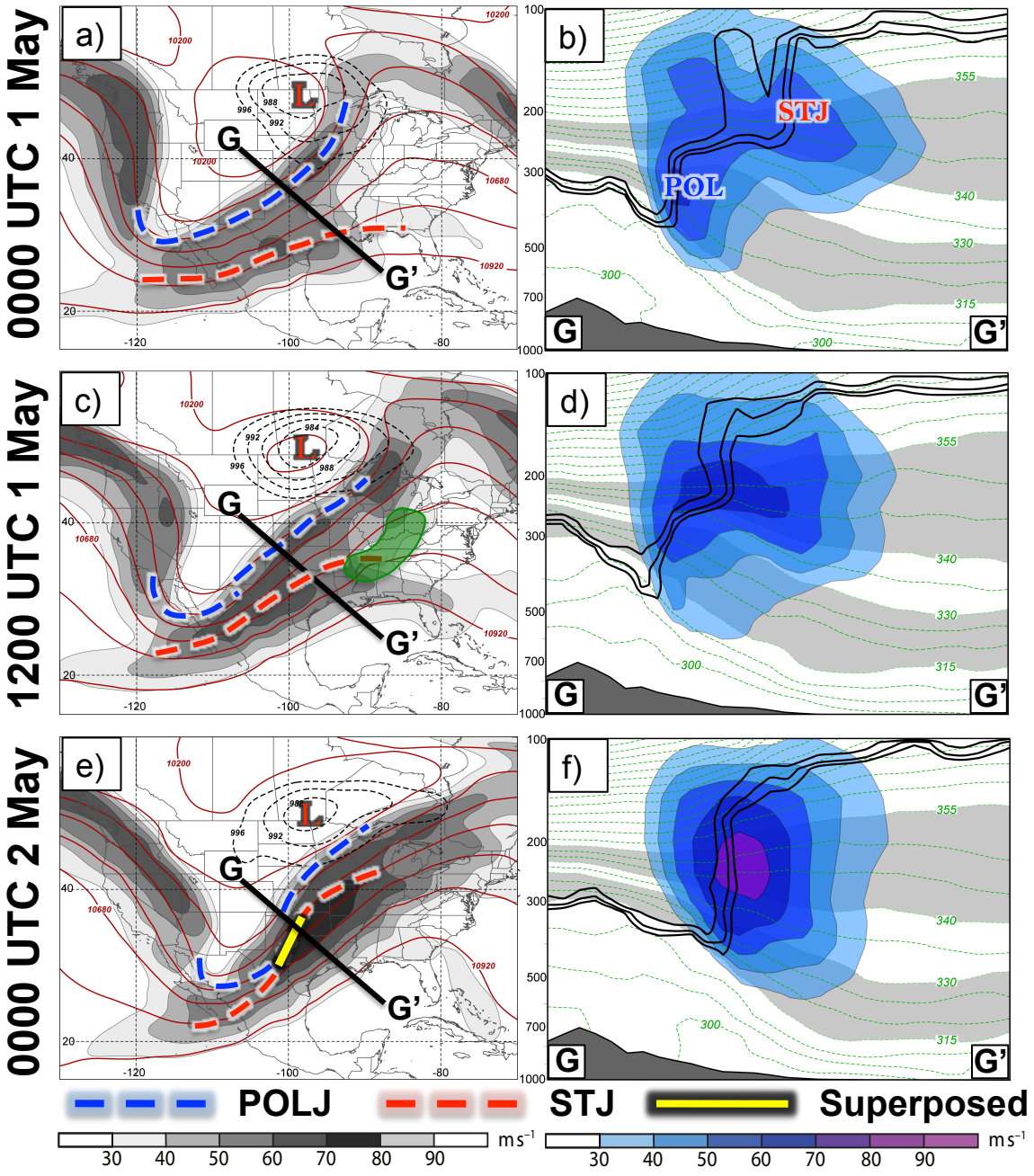

FIG. 12. Conventions are identical to Fig. 5 but for (a,b) 0000 UTC 1 May 2010, (c,d) 1200 UTC 1 May 2010, and (e,f) 0000 UTC 2 May 2010. The precipitation shield at 1200 UTC 1 May 2010 in (c) is denoted by the green shading and sea level pressure is now contoured every 4 hPa below 996 hPa in the left column.

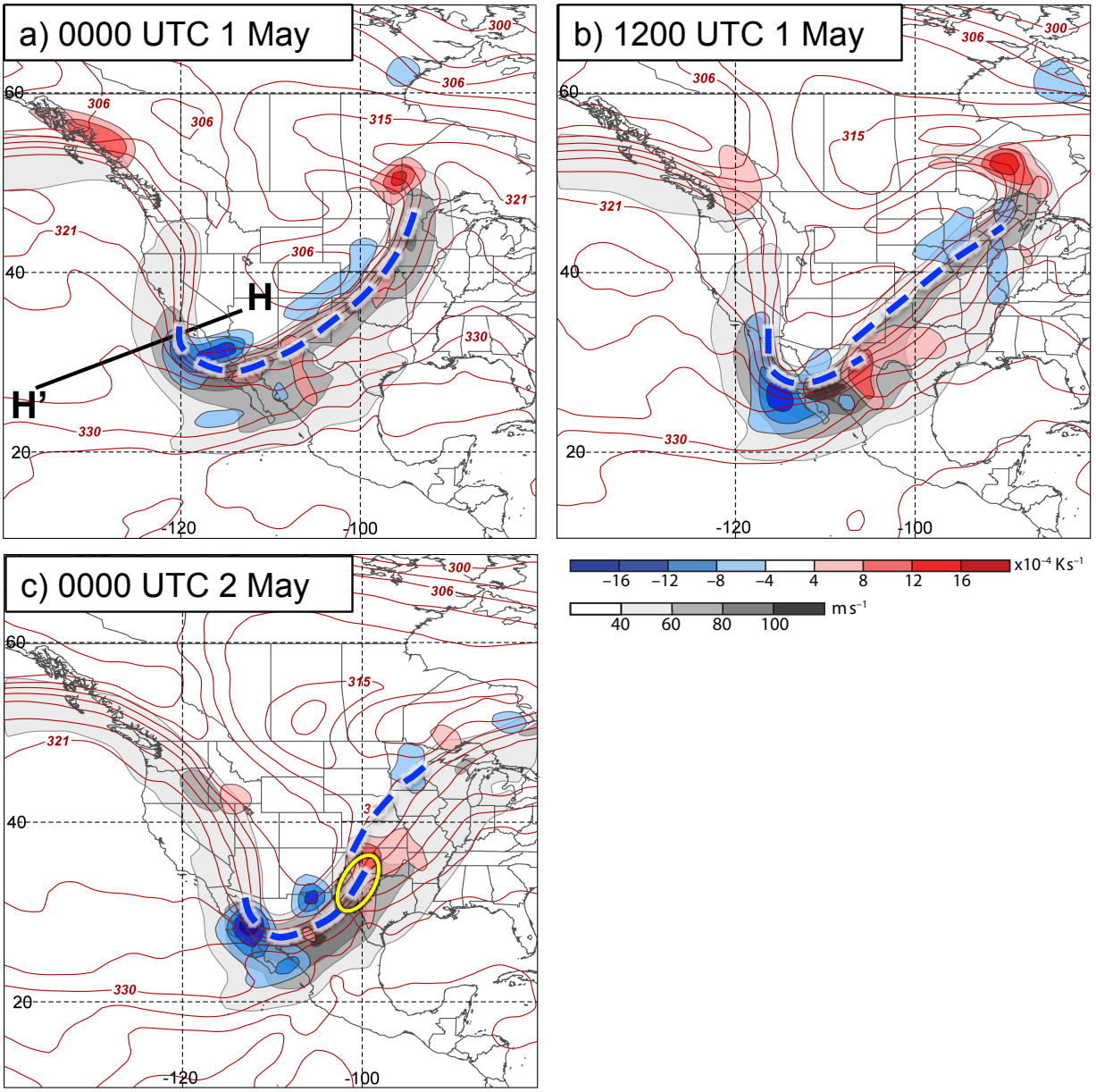

FIG. 13. 300 hPa geostrophic wind speed is shaded in the gray fill pattern according to the legend, 300 hPa geostrophic cold (warm) air advection is shaded in the blue (red) fill pattern following the legend, and 400 hPa potential temperature is contoured in red every 3 K at (a) 0000 UTC 1 May 2010, (b) 1200 UTC 1 May 2010, and (c) 0000 UTC 2 May 2010. Polar jet axes from Fig. 12 are indicated by the thick, blue dashed lines and the yellow circle highlights the region of jet superposition.

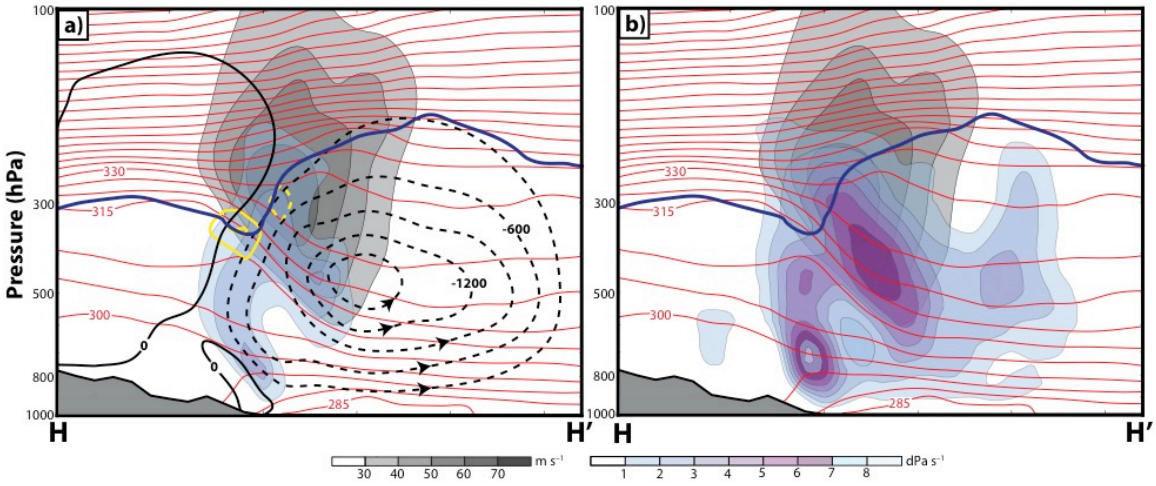

FIG. 14. Conventions are identical to those in Fig. 10, but for the cross section shown in Fig. 13a.

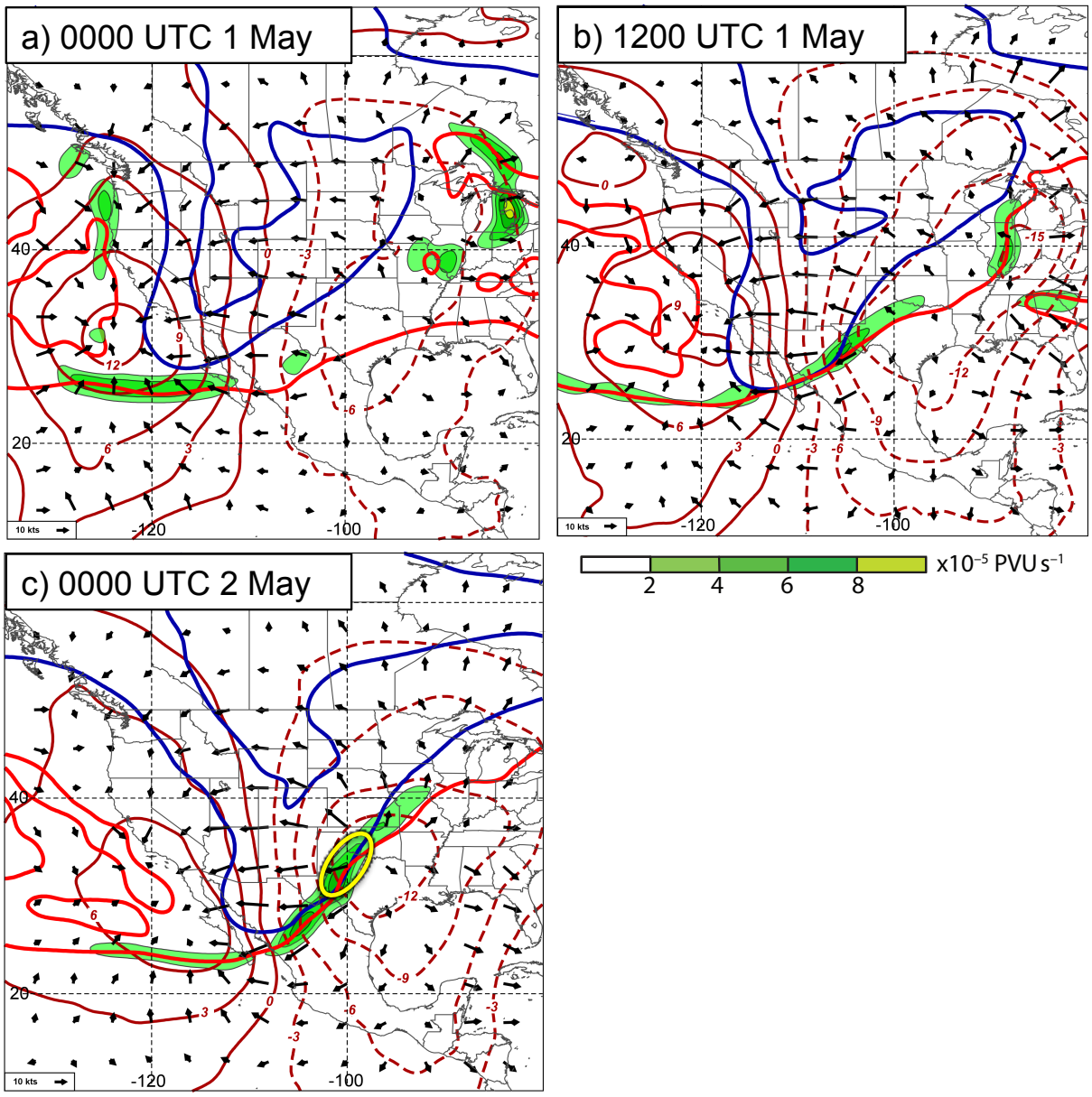

FIG. 15. 200 hPa velocity potential is contoured every $3x10^6$ m^2 s^{-1} with positive (negative) values identified with solid (dashed) thick red lines, the 2-PVU contour at 300 hPa (200 hPa) is identified with the thick blue (red) line, and negative PV advection within the 1–3-PVU channel by the divergent wind (arrows) at 200 hPa is shaded in the green fill pattern following the legend at (a) 0000 UTC 1 May 2010, (b) 1200 UTC 1 May 2010, and (c) 0000 UTC 2 May 2010.

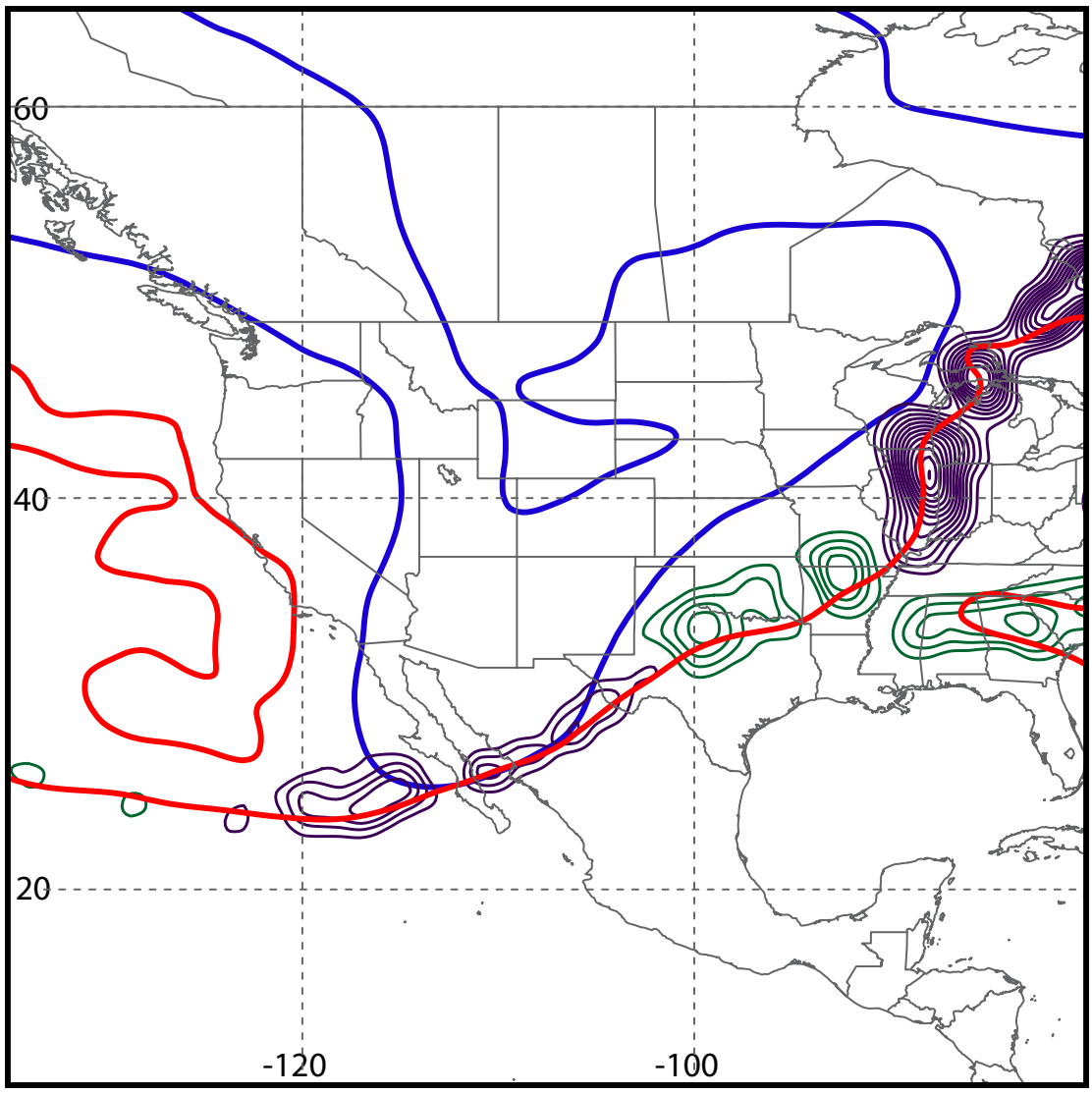

FIG. 16. Conventions are identical to those in Fig. 7, but at 1200 UTC 1 May 2010.

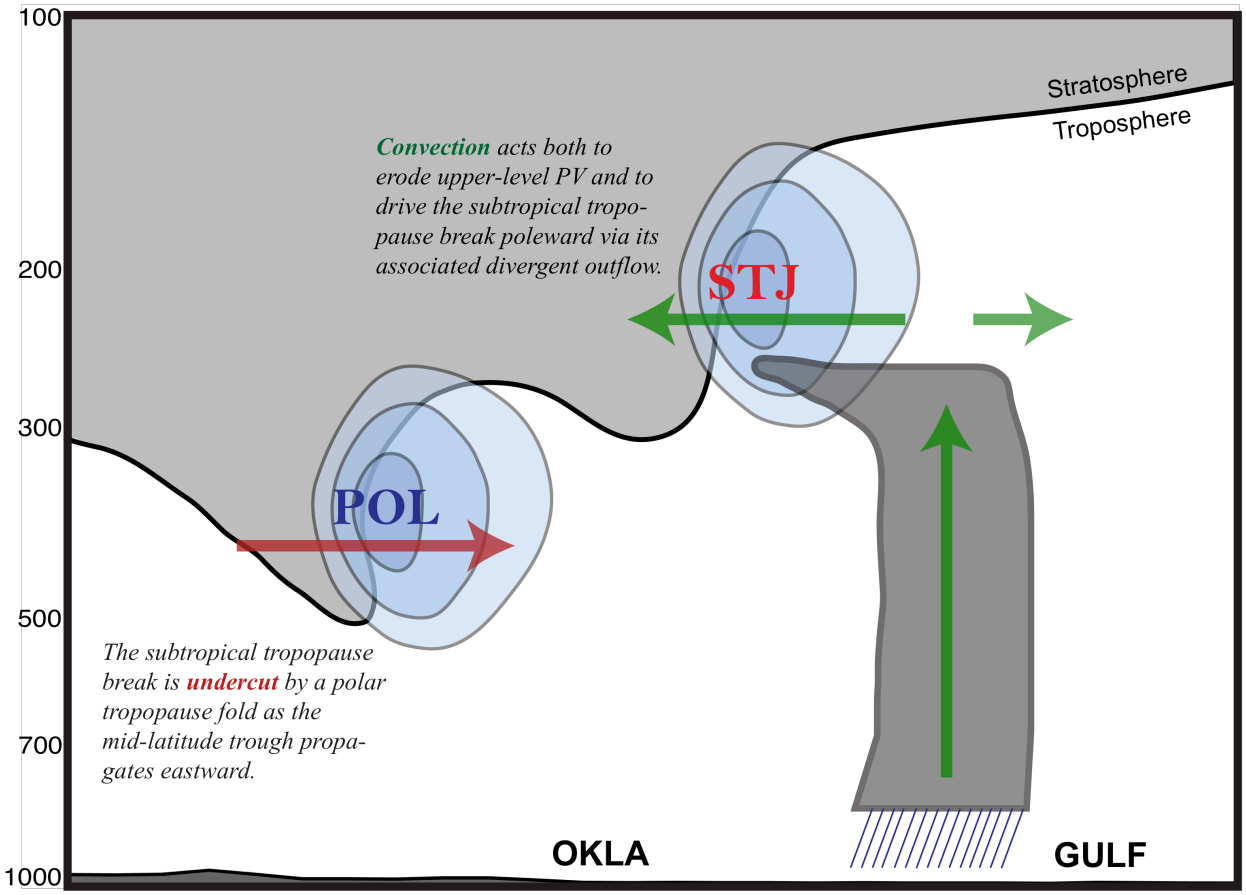

FIG. 17. Conceptual diagram summarizing the development of a superposed jet during the 1–3 May 2010 Nashville Flood. "OKLA" corresponds to Oklahoma and "GULF" denotes the location of the Gulf Coast.